Theoretical and Numerical Analysis of Unsteady Fractional Viscoelastic Flows in Simple Geometries

L.L. Ferrás[a,b,*], Neville J Ford[b], Maria Luísa Morgado[c], Magda Rebelo[d], Gareth H. McKinley[e], João M. Nóbrega[a]

[a] *Institute for Polymers and Composites, University of Minho, Campus de Azurém 4800-058 Guimarães, Portugal*
[b] *Department of Mathematics, University of Chester, CH1 4BJ, UK*
[c] *Centro de Matemática, pólo UTAD, Departamento de Matemática, Universidade de Trás-os-Montes e Alto Douro, UTAD, Quinta de Prados 5001-801, Vila Real, Portugal*
[d] *Centro de Matemática e Aplicações (CMA) and Departamento de Matemática, Faculdade de Ciências e Tecnologia, Universidade NOVA de Lisboa, Quinta da Torre, 2829-516 Caparica, Portugal*
[e] *Department of Mechanical Engineering, Massachusetts Institute of Technology, Cambridge, MA 02139 USA*

Abstract

In this work we discuss the connection between classical and fractional viscoelastic Maxwell models, presenting the basic theory supporting these constitutive equations, and establishing some background on the admissibility of the fractional Maxwell model. We then develop a numerical method for the solution of two coupled fractional differential equations (one for the velocity and the other for the stress), that appear in the pure tangential annular flow of fractional viscoelastic fluids. The numerical method is based on finite differences, with the approximation of fractional derivatives of the velocity and stress being inspired by the method proposed by Sun and Wu for the fractional diffusion-wave equation [Z.Z. Sun, X. Wu, A fully discrete difference scheme for a diffusion-wave system, Applied Numerical Mathematics 56 (2006) 193-209]. We prove solvability, study numerical convergence of the method, and also discuss the applicability of this method for simulating the rheological response of complex fluids in a real concentric cylinder rheometer. By imposing a torsional step-strain, we observe the different rates of stress relaxation obtained with different values of α and β (the fractional order exponents that regulate the viscoelastic response of the complex fluids).

Keywords: Fractional viscoelastic model, annular flows, numerical methods
2000 MSC: ,

1. Introduction

Viscoelastic fluids are abundant in nature, and also play an important role in our daily lives. Examples include coagulating blood [1]; food additives designed for dressing dysphagia [2]; paints that present better or worse adherence to walls; food and plastic products that go through complex

*Corresponding author
Email addresses: luis.ferras@dep.uminho.pt (L.L. Ferrás), njford@chester.ac.uk (Neville J Ford), luisam@utad.pt (Maria Luísa Morgado), msjr@fct.unl.pt (Magda Rebelo), gareth@mit.edu (Gareth H. McKinley), mnobrega@dep.uminho.pt (João M. Nóbrega)

extrusion processes that depend on their rheology, etc. This broad class of fluids often present complex behavior, frequently counterintuitive, that hinders the a priori design of systems in which they are involved. Therefore, it is of major importance to understand the rheological behavior of such a wide variety of complex fluids, allowing, in this way, cost reductions, health improvements, etc.

The recent advances in computational power have led to numerical modeling as a powerful tool for understanding, predicting and optimizing such complex fluid flows [3]. Successful computational analysis requires: (I) the existence of an accurate constitutive model that mimics the physical response of the material under study, and (II) the existence of robust convergent numerical methods for the solution of the resultant complex systems of differential equations [3].

Regarding (I), in the last few years a special class of models has attracted the attention of both engineers and mathematicians. These new models make use of fractional derivatives [4] (integro-differential operators) instead of the classical derivative and classical integral operator. The reason for the success of this class of operators comes from the fact that they can naturally generalise the differential equations governing important physical processes (especially processes with viscoelastic memory), improving their range of applicability and their quantitative ability to describe experimental data (see [4, 5, 6]).

Regarding (II) it is well known that viscoelastic constitutive equations are difficult to solve numerically, especially in complex geometries that include singularities [3], but, nowadays, new methods are being developed that are able to deal with such complexity.

The aim of this work is to address two distinct subjects: *fractional viscoelastic models* and *numerical methods for the solution of a particular set of fractional differential equations*, and thereby to study the unsteady unidirectional flow of fractional viscoelastic fluids inside a real concentric cylinder rheometer (annular flow).

Annular flow between concentric cylinders (including purely tangential, purely longitudinal as well as helical deformation) is not new, and has been addressed in the literature for both classical [7, 8, 9, 10, 11] and fractional viscoelastic models considering the generalised Maxwell [12, 13, 14, 15, 16, 17] and the generalised Oldroyd-B [18, 19, 20, 21, 22, 23, 24] models. Apart from the different fractional models considered, these works differ from each other in the boundary conditions used, and the method in which theoretical results are derived. Most of them present closed form explicit solutions for both velocity and stress, and make use of the Laplace and Hankel transforms to derive the final equations. These transforms pose restrictions on the derivation of the analytical solution (the inverse transforms are only known for a small set of simple functions), and therefore, the solution is limited to specific boundary conditions. Other limitations of the analytical solutions are:

- the infinite series solution is not simple, and the proof of its convergence (when it converges) is not an easy task [13];
- the explicit series solution depends on the roots of a transcendental equation (promoting a decrease in the accuracy of the final solution and making the solution more difficult to obtain) [13, 15].
- the model studied in some analytical works is claimed to come from the simplification of a (unphysical) nonlinear constitutive equation. The model is not frame invariant and this needs to be clarified (see [25, 26]), so that both mathematicians and engineers can continue devel-

oping new fractional constitutive models capable of describing the response of real materials under large straining deformation [13, 15, 23].

In order to overcome these limitations, we develop a numerical method for the solution of the fractional differential equations governing the unidirectional tangential flow of fractional viscoelastic fluids constrained in the annular gap between two coaxial right circular cylinders (the Taylor-Couette geometry). The boundary conditions can be any function of time, and a study of the convergence of the method is provided together with the proof of its solvability. The numerical method is based on finite differences, with the approximation of velocity and stress fractional derivatives, being inspired from the method proposed by Sun and Wu ([27]). It should be remarked that many works can be found in the literature regarding the numerical solution of fractional differential equations. A large proportion of these works is concerned with anomalous diffusion, that can be modeled by having a time fractional derivative with the order of differentiation in the range (0, 1), or, it can be modeled having a space fractional derivative with the order of differentiation in the range (1, 2) (or both). For additional details see the monograph by Podlubny [4], and also [28, 29, 30, 31, 32, 33, 34].

In our case, the time fractional derivative is of order $2-\beta$ with $0<\beta<1$ (for the momentum equation), akin to the fractional diffusion-wave equation, but, we must also include the contribution of a classical time derivative arising from the response of a Newtonian solvent that suspends the complex polymeric additive. For the simplest case of fractional diffusion-wave equations (with no extra classical time derivative) some numerical works can be found in the literature that are helpful in understanding and deriving the numerical method presented in this work. These include the work of Sun and Wu [27] where they present a method based on finite differences with a convergence order of $\mathcal{O}\left(\Delta t^{3-\beta}, \Delta x^2\right)$, (where Δx is the size of the space mesh element and Δt the time step) (see also [35, 36]); the work by Huang et al. [37] where they solve the diffusion-wave equation by transforming it into an equivalent partial integro-differential equation (see also [38]); the work by Zeng [39] where a $\mathcal{O}\left(\Delta t^2, \Delta x^2\right)$ finite difference method is developed; the work by Ding and Li [40] where they develop a finite difference scheme for the fractional diffusion-wave equation with a reaction term, and the work by Murillo and Yuste [41] where they present an explicit method which is shown to be conditionally stable.

Some preliminary results on the pure shear flow of a Fractional Maxwell model were presented at a conference and published in a conference proceeding [42]. The Fractional Maxwell Model is used in that work as an introduction to a more general model, the Fractional K-BKZ model. In the present present work we are concerned only with the Fractional Maxwell Model and we have organised as follows: In order to establish a connection between classical and fractional models we present an introduction to the subject, and also discuss the admissibility of some fractional models proposed in the recent literature (Section 2). The numerical method is presented in Section 3, together with the proof of its solvability and a study of its convergence order. Special attention will also be given to the numerical solution of the tangential annular flow of an Upper Convected Maxwell model. In Section 4 we present a discussion of the effect of the use of the fractional order on the temporal evolution of the velocity and shear stress, and we also present a brief discussion of the stress relaxation obtained for the UCM model. The paper ends with some conclusions in Section 5.

2. The Classical and Fractional constitutive modeling

The most elementary model for the constitutive response of viscoelastic fluids was proposed by Maxwell [9, 43] and is given by $\boldsymbol{\sigma} + \lambda \frac{d\boldsymbol{\sigma}}{dt} = \eta \dot{\boldsymbol{\gamma}}$, with $\boldsymbol{\sigma}$ the stress tensor, $\dot{\boldsymbol{\gamma}} = \left(\nabla \boldsymbol{u} + (\nabla \boldsymbol{u})^T \right)$ the rate of deformation tensor, $\mathbf{u}$ the velocity vector, λ the relaxation time of the fluid and η the viscosity (rate-independent). The model can also be written in integral form as,

$$\boldsymbol{\sigma}(t) = \int_0^t G_0 e^{-\frac{t-t'}{\lambda}} \frac{d\boldsymbol{\gamma}}{dt'} dt' \tag{1}$$

where $G(t) = G_0 e^{\frac{-t}{\lambda}}$ is the relaxation modulus (the response of the stress to a jump in deformation at $t' = 0$), γ is the deformation tensor, and it is assumed that the fluid is at rest for $t < 0$. This is one specific form of the Boltzman integral for linear viscoelastic deformations of complex materials [9].

This type of Maxwell-Debye relaxation (exponential decay) is observed in several complex viscoelastic fluids, but there are other materials showing different types of fading memory, such as an algebraic decay (see for example the work by Keshavarz et al. [44] on biopolymer gels and Ng et al. [45] on bread dough) in which the relaxation modulus is given by,

$$G(t) = St^{-\alpha}, \tag{2}$$

with $0 < \alpha < 1$ and S a scalar measure of the gel strength.

For such materials, if we re-write the relaxation modulus in the form $G(t - t') = \frac{\mathbb{V}}{\Gamma(1-\alpha)} (t - t')^{-\alpha}$ (where $\Gamma(1-\alpha)$ is the gamma function), then, equation (1) can be written as (the physical meaning of $\mathbb{V}$ will be explained later),

$$\boldsymbol{\sigma}(t) = \frac{1}{\Gamma(1-\alpha)} \int_0^t \mathbb{V} \left(t - t'\right)^{-\alpha} \frac{d\boldsymbol{\gamma}}{dt'} dt'. \tag{3}$$

We now introduce the definition of a generalised (fractional) derivative in the Caputo sense. Assuming $0 < \alpha < 1$, the Caputo derivative is given by [46, 47]:

$${}_0^C D_t^\alpha f(t) = \frac{1}{\Gamma(1-\alpha)} \int_0^t \left(t - t'\right)^{-\alpha} \frac{df}{dt'} dt'. \tag{4}$$

The resemblance between equation (3) and the Caputo derivative is evident, therefore the constitutive equation (3) for a material exhibiting power law relaxation of the form in equation (2) can be re-written as $\boldsymbol{\sigma}(t) = \mathbb{V}\, {}_0^C D_t^\alpha \boldsymbol{\gamma}(t)$. Using the compact notation ${}_0^C D_t^\alpha \equiv \frac{d^\alpha}{dt^\alpha}$, we have,

$$\boldsymbol{\sigma}(t) = \mathbb{V} \frac{d^\alpha \boldsymbol{\gamma}(t)}{dt^\alpha}, \tag{5}$$

where $\mathbb{V}$ is a constant for a fixed α, with physical dimensions $Pa.s^\alpha$. $\mathbb{V}$ is a generalised modulus or a *quasi-property*. These quasi-properties are not *true* material properties, like a modulus or viscosity, and are best viewed as the numerical measures of a dynamical process [6, 48]. Note that other fractional derivatives could have been used, such as, for example, the Riemann-Liouville

fractional derivative. The reason for choosing the Caputo derivative is because it allows an easier interpretation of initial conditions and the fact that the Caputo derivative of a constant is 0 [47, 4].

Recognizing that for $\alpha = 1$, $\mathbb{V} = \eta$, and, for $\alpha = 0$, $\mathbb{V} = G_0$, equation (5) can be viewed as a general constitutive relationship to represent a viscous fluid ($\boldsymbol{\sigma}(t) = \mathbb{V}\frac{d^1\boldsymbol{\gamma}(t)}{dt^1}$), an elastic solid ($\boldsymbol{\sigma}(t) = \mathbb{V}\frac{d^0\boldsymbol{\gamma}(t)}{dt^0} = \mathbb{V}\gamma(t)$), and a mix of both states ($\boldsymbol{\sigma}(t) = \mathbb{V}\frac{d^{\boldsymbol{\alpha}}\gamma(t)}{dt^{\alpha}}$, $0 < \alpha < 1$), interpolating between an elastic spring and a viscous dashpot (5). The mechanical response given by equation (5) is often referred to as a Scott Blair element or springpot [49].

A mechanical interpretation in terms of classical springs and dashpots was derived by Schiessel and Blumen [50] (see also [51, 52]), where the fractional model can be seen as an infinite series-parallel combination of springs and dashpots (resulting in the so-called *springpot*), as shown in figure 1(a).

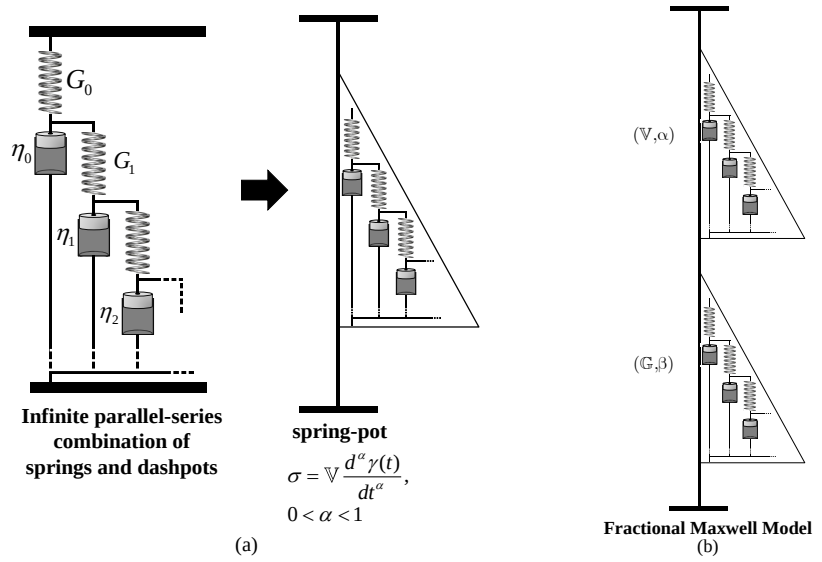

Figure 1: (a) Infinite combination of springs and dashpots leading asymptotically to the concept of a springpot. (b) Fractional Maxwell model (a combination of two springpots in series).

Definition 2.1. *Fractional Maxwell model (FMM)*
Following Schiessel and Blumen [50], and using the notation of [6, 26] the FMM is given by a representation of two springpots arranged in series, as shown in figure 1(b). Assuming that the stress felt by each springpot is the same ($\sigma(t) = \mathbb{V}\frac{d^{\alpha}\gamma_1(t)}{dt^{\alpha}} = \mathbb{G}\frac{d^{\beta}\gamma_2(t)}{dt^{\beta}}$), and that the total deformation is given by $\gamma(t) = \gamma_1(t) + \gamma_2(t)$, then the fractional differential equation representing the relationship between tensorial stress and deformation is given by,

$$\boldsymbol{\sigma}(t) + \frac{\mathbb{V}}{\mathbb{G}}\frac{d^{\alpha-\beta}\boldsymbol{\sigma}(t)}{dt^{\alpha-\beta}} = \mathbb{V}\frac{d^{\alpha}\boldsymbol{\gamma}(t)}{dt^{\alpha}}, \tag{6}$$

where it has been assumed (without loss of generality) that $0 < \beta \leq \alpha < 1$.

This four parameter linear viscoelastic model is able to describe a much wider range of complex fluid behavior when compared to the classical Maxwell model (obtained in the limit $\alpha = 1, \beta = 0$). It is not difficult to imagine that a representative of a complex material element, may be

subjected to a wide range of different relaxation processes when deformed (due to the wide range of underlying molecular constituents). When using the classical Maxwell model we only capture a single characteristic relaxation time, whereas by using the FMM a wide spectrum of different relaxation processes are considered (corresponding to figure 1(c)). Note that for this model we have four parameters (two quasiproperties $\mathbb{V}$, $\mathbb{G}$ and two fractional exponents) that need to be determined from regression to experimental data.

Typical values of the quasiproperties and fractional exponents are $\mathbb{V} \in [0.12,\ 48]\ Pa.s^{\alpha}$, $\mathbb{G} \in [0.12,\ 5.4]\ Pa.s^{\beta}$, $\alpha \in [0.73,\ 0.92]$, $\beta \in [0.23,\ 0.39]$, for the xanthan gum based food-thickening dysphagia product Resource ® Thicken Up Clear (a benchmark food additive system designed to produce fluids with specific food textures at appropriate concentrations) produced by Nestlé [2]. (The different values of $\mathbb{V}, \mathbb{G}, \alpha$ and β come from different concentrations of Thicken Up Clear that were used, 0.1 to 4.5 $[wt.\%]$); $\mathbb{V} \in [7.02,\ 208.54]\ Pa.s^{\alpha}$, $\mathbb{G} \in [1.82,\ 22.46]\ Pa.s^{\beta}$, $\alpha \in [0.60,\ 0.76]$, $\beta \in [0.14,\ 0.24]$ for a different system composed of aqueous solutions of xanthan gum [26] in water with a concentration ranging from 0.25 to 1 $[wt.\%]$ (for both cases the α and β values decrease with increasing concentration). For other food gums such as guar gum (0.5 $wt.\%$) $\mathbb{V} = 0.74\ Pa.s^{\alpha}$, $\mathbb{G} = 7.9\ Pa.s^{\beta}$, $\alpha = 0.83$, $\beta = 8.2 \times 10^{-2}$; for tara gum (0.4 $wt.\%$) $\mathbb{V} = 0.18\ Pa.s^{\alpha}$, $\mathbb{G} = 8.7\ Pa.s^{\beta}$, $\alpha = 0.92$, $\beta = 0$ [2].

In general, assuming $0 < \beta < \alpha < 1$, it can be shown that in the linear viscoelastic regime following a step strain displacement the exponent α captures the slope $d\log(G(t))/dt$ at long time intervals (or low frequencies), and the exponent β captures the slope at short time intervals (or high frequencies) [26, 53, 54].

The FMM (equation (6)) shows unbounded stress growth following start up of steady shear with a deformation of the form $\dot{\gamma} = \dot{\gamma}_0 H(t)$ (where $H(t)$ is the Heaviside step function and $\dot{\gamma}_0$ is the rate of shearing strain), or equivalently, the transient viscosity $\eta^{+}(t) = \lim_{t\to\infty} \sigma(t)/\dot{\gamma}_0$ diverges at long times. To prevent unbounded stress growth and have a finite zero shear viscosity, η_0, as expected for a viscoelastic fluid, we require $\alpha = 1,\ \mathbb{V} = \eta_0$.

The resulting three parameter model can be written in the form

$$\boldsymbol{\sigma}(t) + \frac{\mathbb{V}}{\mathbb{G}} \frac{d^{1-\beta}\boldsymbol{\sigma}(t)}{dt^{1-\beta}} = \mathbb{V}\frac{d\boldsymbol{\gamma}(t)}{dt}, \tag{7}$$

and we refer to this as the Fractional Viscoelastic Fluid model (FVF) (see figure 2).

The supremacy of the FVF over the classical Maxwell model in describing relaxation data of complex fluids can be seen for example in figure 2, where we show the fit to the relaxation modulus obtained after applying a step strain of the form $\gamma = \gamma_0 H(t)$. The experimental data was obtained for a polydimethylsiloxane sample [55] and a nonlinear regression was used to perform the fit. Note that a corresponding fit with a multimode Maxwell model requires $N = 5$ modes (or 10 parameters) to achieve a similar level of fidelity.

For this three parameter model (FVF) the storage and loss moduli in small amplitude oscillatory shear flows (SAOS) with $\dot{\gamma} = \gamma_0 \omega \cos(\omega t)$ are given by [6],

$$\begin{aligned} G'(\omega) &= \frac{(\mathbb{V}\omega)^2 \mathbb{G}\omega^{\beta} \cos\left(\frac{\pi}{2}\beta\right)}{(\mathbb{V}\omega)^2 + \left(\mathbb{G}\omega^{\beta}\right)^2 + 2\mathbb{V}\omega\mathbb{G}\omega^{\beta}\cos\left(\frac{\pi}{2}(1-\beta)\right)} \\ G''(\omega) &= \frac{\left(\mathbb{G}\omega^{\beta}\right)^2 \mathbb{V}\omega + (\mathbb{V}\omega)^2 \mathbb{G}\omega^{\beta}\sin\left(\frac{\pi}{2}\beta\right)}{(\mathbb{V}\omega)^2 + \left(\mathbb{G}\omega^{\beta}\right)^2 + 2\mathbb{V}\omega\mathbb{G}\omega^{\beta}\cos\left(\frac{\pi}{2}(1-\beta)\right)} \end{aligned} \tag{8}$$

The crossover frequency, ω_c, at which $G' = G''$ is then given by equating these expressions to give,

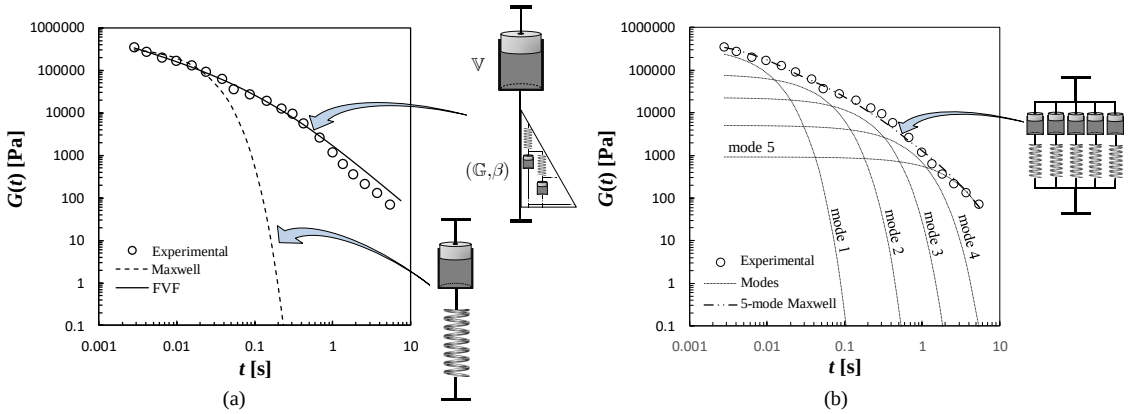

Figure 2: Fit of a single mode Maxwell model (spring-dashpot) and the three parameter FVF (springpot-dashpot) to the experimental relaxation modulus data of a polydimethylsiloxane sample (the experimental data was adapted from [55]). The fitting parameters are $\mathbb{V} = 1.73 \times 10^4\ Pa.s$, $\mathbb{G} = 4.45 \times 10^4\ Pa.s^{\beta}$ and $\beta = 4.63 \times 10^{-1}$ for the FVF, and, $G_i = \eta_i \lambda_i = 3.59 \times 10^5\ Pa$, $\lambda_i = 1.55 \times 10^{-2}\ s$ for the Maxwell model. (b) Fit performed using a 5-mode Maxwell model ($G_i = \eta_i \lambda_i = 3.50{\times}10^5$, $8.01{\times}10^4$, $2.30{\times}10^4$, $5.00{\times}10^3$, $9.20{\times}10^2\ Pa$; $\lambda_i = 7.00 \times 10^{-3}$, $4.00{\times}10^{-2}$, $1.5{\times}10^{-1}$, 0.5, 2 s).

$$\omega_c = \left(\frac{\mathbb{G}}{\mathbb{V}} \left[\frac{1}{\cos\left(\frac{\pi}{2}\beta\right) - \sin\left(\frac{\pi}{2}\beta\right)} \right] \right)^{\frac{1}{1-\beta}}. \tag{9}$$

Note that for $\beta \to 0.5$ the crossover frequency diverges, and for $\beta > 0.5$, ω_c is not defined because $\cos\left(\frac{\pi}{2}\beta\right) - \sin\left(\frac{\pi}{2}\beta\right) < 0$. Neglecting the algebraic correction given by this term, quite generally a characteristic time scale for the FVF can be given by $\tau \approx (\mathbb{V}/\mathbb{G})^{1/(1-\beta)}$ [6, 26]. For the data shown in figure 2(a) $\tau = 0.172\ s$.

Since the FMM has four model parameters, it is expected to provide additional flexibility in fitting a wider range of complex fluid rheology, particularly for complex fluids such as biopolymer gels for which the zero shear viscosity is indeed unbounded. In order to test this, we have performed a fit with a Maxwell model and both FMM and FVF to the experimental data (G' and G'') obtained from the rheological characterisation (Small Amplitude Oscillatory Shear at 230 °C) of a polystyrene extrusion grade, Polystyrol 158K from BASF [56], and the experimental data obtained for the xanthan gum with a concentration of 0.25 $wt.\%$ [26] (presented before).

From the results shown in figure 3, it can be seen that using $\alpha \neq 1$ as an additional model parameter, a slightly better fit is obtained (see the region inside the dashed rectangle). To quantify the error incurred during the fitting process we will use a mean square error given by (see [55]-Appendix3A and [57]),

$$\varepsilon = \sum_i \left[\log G_i^{'} - \log G_{fit}^{'}(\omega_i) \right]^2 + \sum_i \left[\log G_i^{''} - \log G_{fit}^{''}(\omega_i) \right]^2. \tag{10}$$

Numerical values for each set of fitted parameters are given in each part of figure (3). Comparing the fractional model fit with the fit obtained with the Maxwell model, we see that using a combination of a springpot and dashpot, or, a combination of two springpots, leads to huge

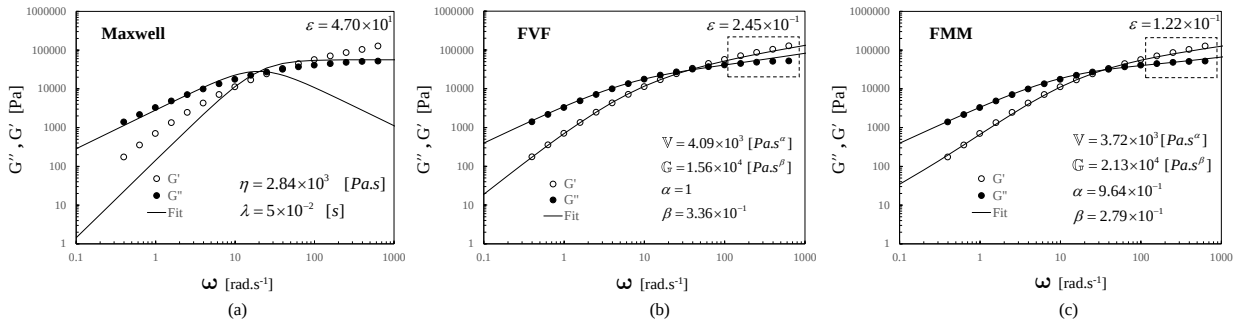

Figure 3: Fit of the elastic and viscous contributions G' and G'' to the linear viscoelastic modulus obtained from the rheological characterisation of a polystyrene extrusion grade, Polystyrol 158K from BASF using (a) Maxwell model; (b) FVF; (c) FMM.

improvements in modeling real data. For the FVF we obtain $\omega_c = 34.7\ s^{-1}$, $\frac{1}{\omega_c} = 2.88 \times 10^{-2}$ s, $\tau \approx (\mathbb{V}/\mathbb{G})^{1/(1-\beta)} = 1.34 \times 10^{-1}\ s$.

For the xanthan gum [26] with a concentration of 0.25 $wt.\%$, the quality of the fit obtained with the FVF (figure 4) is less ($\varepsilon = 3.48 \times 10^{-1}$) when compared to the fit obtained for the Polystyrol 158K ($\varepsilon = 2.45 \times 10^{-1}$); however, the fit quality is still really good, especially when compared to the poor fit obtained with the Maxwell model ($\varepsilon = 4.70 \times 10^{1}$). Note that the results presented in (figure 4(d)) were obtained from [26].

We have also compared the performance of the FVF with another three parameter model, the Jeffreys model [58, 9, 43]. We see that the fitting error is much smaller in the FVF ($\varepsilon_{FVF} \ll \varepsilon_{Jeffreys}$). The conclusion is that the FVF although requiring one less parameter when compared to FMM, is still adequate to model the rheological behavior of different viscoelastic fluids, unless very high precision is needed in the high frequency regime, while also having the benefit of a well defined steady shear viscosity η_0 in the limit of long times $t \gg \tau$.

2.1. Admissible Models

All of these linear viscoelastic models suffer from a serious problem, they are not frame-invariant [64]. Although rheological invariance is by no means a simple subject, it is sufficient to note here that the description of physical phenomena should remain unchanged, if we change the point of view of the observer (the frame of reference), and the material properties should be independent of the observer [59, 60, 61]. Therefore the mathematical formulas that represent physical phenomena should reflect this invariance.

The classic Maxwell model can be improved to become frame-invariant. The resulting model is known as the Upper Convected Maxwell (UCM) model [62, 59, 9, 63], and is given by $\boldsymbol{\sigma} + \lambda \overset{\nabla}{\boldsymbol{\sigma}} = \eta \left(\nabla \mathbf{u} + (\nabla \mathbf{u})^T \right)$ where $\overset{\nabla}{\boldsymbol{\sigma}} = \left\{ \frac{\partial \boldsymbol{\sigma}}{\partial t} + \mathbf{u}.\nabla\boldsymbol{\sigma} - (\nabla \mathbf{u})^T.\boldsymbol{\sigma} - \boldsymbol{\sigma}.\nabla\mathbf{u} \right\}$ is the upper convected derivative. In the literature, several publications can be found regarding the so called *fractional Upper Convected Maxwell* model (see for example [13, 21]), where, the time derivative of the stress, in the UCM model, is substituted by a fractional derivative, $\overset{\nabla}{\boldsymbol{\sigma}}_{\zeta} = \left\{ \frac{d^{\zeta}\boldsymbol{\sigma}(t)}{dt^{\zeta}} + \mathbf{u}.\nabla\boldsymbol{\sigma} - (\nabla \mathbf{u})^T.\boldsymbol{\sigma} - \boldsymbol{\sigma}.\nabla\mathbf{u} \right\}$ with $0 < \zeta < 1$.

However, one cannot just simply substitute one derivative by the other, since, we need to be sure that the equation is frame-invariant [64] (additionally, this proposed equation is dimensionally

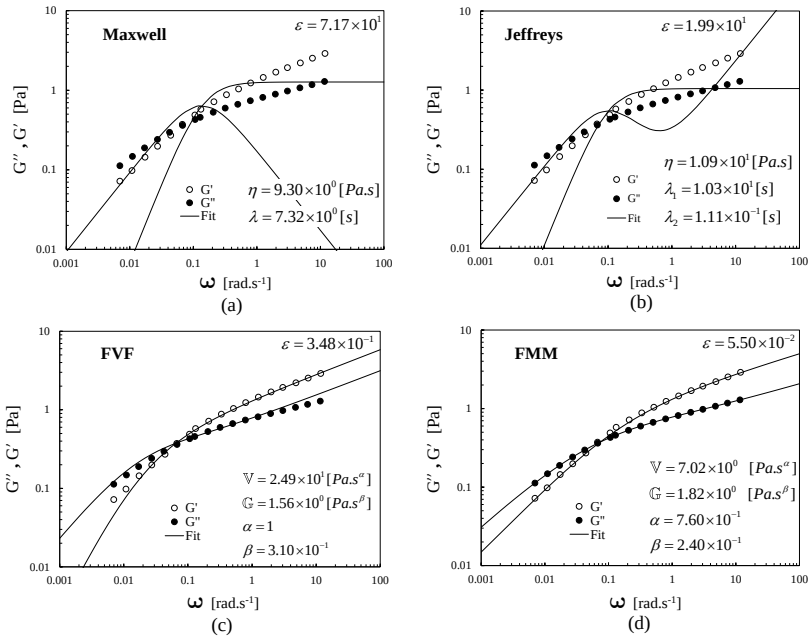

Figure 4: Fit of G' and G'' data for an aqueous xanthan gum solution from [26]. (a) Maxwell model; (b) 3 parameter Jeffreys model; (c) 3 parameter FVF; (d) 4 parameter FMM (parameters given by [26]).

inconsistent). Therefore, these works present a model that cannot be considered a true nonlinear constitutive equation (see [65, 66, 67, 68] and [60] pp. 222-223). For a discussion on frame-invariant fractional constitutive equations please see the work by Pan Yang et al. [64] and the references cited therein. Note that this is a recent and difficult subject (frame-invariant fractional models), and that few works can be found in the literature regarding this subject [25].

Accordingly, the objective of the present work is to study the FMM and FVF by considering specific flows where they become physically acceptable constitutive equations, that is, flows in which the material response remains in the Linear Viscoelastic (LVE) regime. This LVE regime can be easily understood in context of a Pipkin diagram [69] shown in figure 5, where the various regimes exhibited by viscoelastic liquids in oscillatory flow are presented. By defining the Deborah and Weissenberg numbers as $De = \tau\omega$ and $Wi = De\gamma_0$, respectively, we then conclude that the FMM and the FVF are valid for time varying flows at arbitrary frequencies providing the strain amplitude is sufficiently small that $Wi \ll 1$ (gray region of figure 5).

We therefore consider in this work the startup of linear shear flows at small enough strains, so that the fluid response is linear. In the future we will consider more complex frame invariant models [25, 64] that also enable description of non-linear viscoelasticity (patterned region in figure 5).

2.2. Taylor-Couette Flow

Coaxial annular flow in which a fluid is confined between two cylinders (see figure 6), has been studied for a long time [70, 71, 72, 73]. Maurice Couette described this arrangement in his thesis (1890), and, for a historical review see [74, 75, 76]. This type of flow has the particular importance

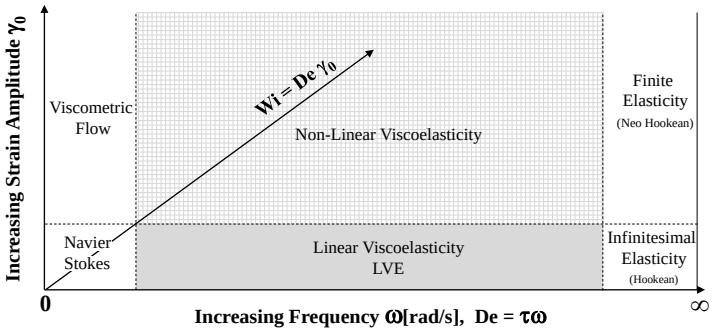

Figure 5: Schematic of the Pipkin diagram.

of allowing the rheological characterisation of materials by loading the unknown material into the annular gap (see figure 6), rotating one cylinder (in a steady or unsteady motion) and measuring the resulting torque on the second cylindrical surface [76].

The tangential component of the governing momentum equation in terms of u_θ ($\theta - component$ of the momentum equation), and shear stress, $\sigma_{r\theta}$, for this pure tangential annular flow with an imposed velocity profile $(u_r, u_\theta, u_z) = (0, u_\theta(r,t), 0)$, are given by

$$\begin{aligned} \rho\left(1+\lambda\tfrac{\partial}{\partial t}\right)\tfrac{\partial u_\theta}{\partial t} &= \eta\left(\tfrac{\partial^2}{\partial r^2}+\tfrac{1}{r}\tfrac{\partial}{\partial r}-\tfrac{1}{r^2}\right)u_\theta \\ \left(1+\lambda\tfrac{\partial}{\partial t}\right)\sigma_{r\theta} &= \eta\left(\tfrac{\partial u_\theta}{\partial r}-\tfrac{u_\theta}{r}\right) \end{aligned} \tag{11}$$

for the Maxwell model. See Appendix A for the derivation of these equations. Note that the same operator $\left(1+\lambda\frac{\partial}{\partial t}\right)$ arises in both equations. This operator comes from the constitutive response of the shear stress (see Appendix A).

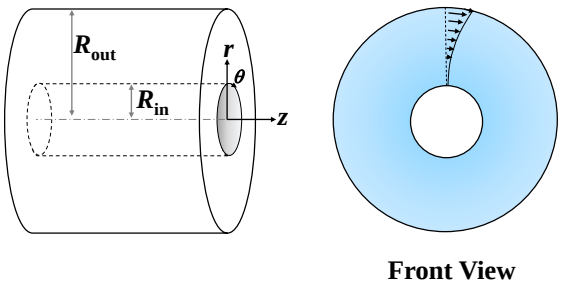

Figure 6: Schematic of the annular geometry and flow (R_{in} and R_{out} represent the radii of the inner and outer cylinders, respectively). Here only the outer cylinder is rotated.

The generalisation to a fractional viscoelastic fluid (FVF) response at small $Wi(\ll 1)$ can be obtained by changing the operator $\left(1+\lambda\frac{\partial}{\partial t}\right)$ to the fractional derivative $\left(1+\frac{\mathbb{V}}{\mathbb{G}}D_t^{1-\beta}\right)$ in equation (11), leading to:

$$\rho\left(1+\frac{\mathbb{V}}{\mathbb{G}}D_t^{1-\beta}\right)\frac{\partial u_\theta}{\partial t} = \mathbb{V}\left(\frac{\partial^2}{\partial r^2}+\frac{1}{r}\frac{\partial}{\partial r}-\frac{1}{r^2}\right)u_\theta, \tag{12}$$

$$\sigma_{r\theta} + \frac{\mathbb{V}}{\mathbb{G}} D_t^{1-\beta} \sigma_{r\theta} = \mathbb{V} \left(\frac{\partial}{\partial r} - \frac{1}{r} \right) u_\theta. \tag{13}$$

We next consider how to discretise and solve these equations numerically.

3. Numerical Method

This Section is dedicated to the discretisation and numerical solution of equations (12) and (13). To test the convergence of the method we compare the numerical results obtained, with the existing analytical solution for the Newtonian case; we develop a numerical code developed for the solution of annular UCM flows, and compare the results obtained from the different numerical methods (considering the fractional model converging to the UCM constitutive equation); finally we study the convergence order of the method by comparing the numerical results with generalised analytical solutions.

3.1. Discretisation of the Velocity and Shear stress Equations

In this subsection we will derive a numerical method for the solution of the system of fractional partial differential equations (12) and (13), with boundary and initial conditions of Dirichlet type:

$$u_\theta(R_{in}, t) = \phi_i(t), \; u_\theta(R_{out}, t) = \phi_o(t), \quad 0 < t < T, \tag{14}$$

$$u_\theta(r, 0) = \frac{\partial u_\theta(r, 0)}{\partial t} = 0, \; \sigma_{r,\theta}(r, 0) = 0, \qquad R_{in} < r < R_{out}, \tag{15}$$

Physically the latter condition corresponds to a viscoelastic fluid at rest and fully relaxed at $t = 0$. In order to solve the system of equations (12, 13) numerically, we need to obtain an approximation for all the operators (time and spatial derivatives). For that, we consider a uniform space mesh on the interval $[R_{in}, R_{out}]$, defined by the gridpoints $r_i = R_{in} + i\Delta r$, $i = 0, \ldots, N$, where $\Delta r = \frac{R_{out} - R_{in}}{N}$. For the discretisation of the fractional time derivative we also assume a uniform mesh, with a time step $\Delta t = T/S$ and time gridpoints $t_s = s\Delta t$, $s = 0, 1, ..., S$.

The single fractional differential equation governing the evolution of velocity in both time and space, developed by eliminating the shear stress from the tangential component of the momentum equation can be re-written as:

$$\frac{\rho}{\mathbb{V}} \frac{\partial u_\theta}{\partial t} + \frac{\rho}{\mathbb{G}} D_t^{2-\beta} u_\theta = \frac{\partial^2 u_\theta}{\partial r^2} + \frac{1}{r} \frac{\partial u_\theta}{\partial r} - \frac{u_\theta}{r^2} \tag{16}$$

The numerical method to solve equation (16) is based on the method presented by Sun and Wu [27] for the fractional diffusion-wave equation.
Denoting by u_i^s an approximation of $u_\theta(r_i, t_s)$, $i = 1, ..., N-1$, $s = 1, ..., S$ we can define the following:

$$u_i^{s-1/2} \equiv \frac{1}{2} \left(u_i^s + u_i^{s-1} \right) \tag{17}$$

$$\delta_t u_i^{s-1/2} \equiv \frac{1}{\Delta t} \left(u_i^s - u_i^{s-1} \right) \tag{18}$$

$$\delta_r u_{i-1/2}^s \equiv \frac{1}{\Delta r}\left(u_i^s - u_{i-1}^s\right) \tag{19}$$

$$\delta_r^2 u_i^s \equiv \frac{1}{\Delta r}\left(\delta_r u_{i+1/2}^s - \delta_r u_{i-1/2}^s\right) \tag{20}$$

Each term of equation (16) is then substituted by its respective finite difference approximation at mesh point r_i, that is, $\frac{\partial u_\theta}{\partial t} \approx \delta_t u_i^{s-1/2}$, $\frac{\partial^2 u_\theta}{\partial r^2} \approx \delta_r^2 u_i^{s-1/2}$, $\frac{1}{r}\frac{\partial u_\theta}{\partial r} \approx \frac{1}{4r_i}\left(\delta_r u_i^s + \delta_r u_i^{s-1}\right)$, $\frac{u_\theta}{r^2} \approx \frac{u_i^{s-1/2}}{r_i^2}$. Note that these approximations come from an average in time (a well known procedure for increasing the accuracy of the method [27]). The numerical approximation to the fractional derivative, $D_t^{2-\beta}$, is given by [27],

$$\begin{array}{l} \frac{1}{\Gamma(2-\epsilon)}\int_0^{t_s}\left(t_s - t'\right)^{1-\epsilon}\frac{d^2 u_\theta(t')}{dt'^2}dt' \approx \\ \quad \approx \frac{1}{\Delta t\Gamma(2-\epsilon)}\left[a_0\delta_t u_i^{s-1/2} - \sum_{j=0}^{s-1}\left(a_{n-j-1} - a_{n-j}\right)\delta_t u_i^{j-1/2} + \frac{\partial u_\theta(r_i,0)}{\partial t}\right] \end{array} \tag{21}$$

with

$$a_l = \int_{t_l}^{t_{l+1}} \frac{1}{t^{\epsilon-1}}dt = \frac{(\Delta t)^{2-\epsilon}}{2-\epsilon}\left[(l+1)^{2-\epsilon} - l^{2-\epsilon}\right],\ l \geq 0. \tag{22}$$

and $\epsilon = 2 - \beta$.

The discretized velocity equation can then be written as,

$$\begin{array}{ll} \frac{\rho}{\mathbb{V}}\delta_t u_i^{s-1/2} & + \frac{\rho}{\Gamma(\beta)\mathbb{G}}\frac{1}{\Delta t}\left[a_0\delta_t u_i^{s-1/2} - \sum_{j=0}^{s-1}\left(a_{n-j-1} - a_{n-j}\right)\delta_t u_i^{j-1/2}\right] \\ & = \delta_r^2 u_i^{s-1/2} + \frac{1}{2r_i}\left(\frac{\delta_r u_i^s + \delta_r u_i^{s-1}}{2}\right) - \frac{u_i^{s-1/2}}{r_i^2} \end{array} \tag{23}$$

for $i = 1, ..., N-1$ and $s = 1, ..., S$.

At each of the cylinder boundaries we have $u_0^s = \phi_0\left(s\Delta t\right)$ and $u_N^s = \phi_N\left(s\Delta t\right)$. This will generate (at each time step) a linear system of $(N-1)\times(N-1)$ algebraic equations for $(N-1)\times(N-1)$ unknowns. For a better understanding of the approximations used to discretise the velocity equation the work by Sun and Wu [27] should be consulted (the numerical results that will be shown later suggest the convergence order expected for this method).

After solving the system of equations, an approximation of velocity at time and space mesh points is known, and, the evolution shear stress equation, Eq. (13), can be solved separately. It should be remarked that the right-hand-side of Eq. (13) is known and therefore we only need to this equation in time with initial condition $\sigma_{r\theta}(r, 0) = 0$.

Denoting by σ_i^s an approximation of $\sigma_{r\theta}\left(r_i, t_s\right)$, the discretised equation for the evolution of the shear stress can be written as:

$$\sigma_i^s \quad + \frac{\mathbb{V}}{\Gamma(\beta)\mathbb{G}}\frac{1}{\Delta t}\left[b_0\sigma_i^s - \sum_{j=0}^{s-1}\left(b_{n-j-1} - b_{n-j}\right)\sigma_i^j\right] = \mathbb{V}\left[\left(\frac{u_{i+1}^s - u_{i-1}^s}{2\Delta r}\right) - \frac{u_i^s}{r_i}\right] \tag{24}$$

for $i = 1, ..., N-1$ and $s = 1, ..., S$ with,

$$b_l = \int_{t_l}^{t_{l+1}} \frac{1}{t^\Theta}dt = \frac{(\Delta t)^{1-\Theta}}{1-\Theta}\left[(l+1)^{1-\Theta} - l^{1-\Theta}\right],\ l \geq 0. \tag{25}$$

and $\Theta = 1 - \beta$.

Again, the approximation used for each term in equation (13) is obvious, when comparing Eqs. (13) and (24). A second order approximation was used to approximate $\frac{\partial u_\theta}{\partial r}$. It should be remarked that in this equation we do not need to provide boundary conditions for the stress but we do need an initial condition.

Note that the operator used to approximate the fractional derivative appearing in the velocity equation, Eq. (16) is not the same as the one used in the stress equation, Eq. (13). The main difference is that the order of the fractional derivative for the velocity equation is $2-\beta$ while the order of the fractional derivative in the stress equation is $1-\beta \in (0,1)$.

The right-hand-side of equation (24) comes from equation (23), and at each time step ($s\Delta t$, $s = 1, ..., S$) equations (23) and (24) are solved sequentially (in this order).

3.1.1. Solvability

For $s = 1, 2, ..., S$ and $i = 1, 2, ..., N-1$ we may rewrite equation (23) as:

$$\begin{aligned}\frac{\rho}{\mathbb{V}}\frac{1}{\Delta t}\left(u_i^s - u_i^{s-1}\right) \quad &+\frac{\rho}{\Gamma(\beta)\mathbb{G}}\frac{1}{\Delta t}\left[a_0\frac{1}{\Delta t}\left(u_i^s - u_i^{s-1}\right) - \sum_{j=0}^{s-1}\left(a_{n-j-1} - a_{n-j}\right)\frac{1}{\Delta t}\left(u_i^j - u_i^{j-1}\right)\right] = -\frac{\left(u_i^s + u_i^{s-1}\right)}{2r_i^2} \\ &+\frac{1}{(\Delta r)^2}\left[\left(\frac{u_{i+1}^s + u_{i-1}^s}{2}\right) - u_i^s + \left(\frac{u_{i+1}^{s-1} + u_{i-1}^{s-1}}{2}\right) - u_i^{s-1}\right] + \frac{1}{2r_i\Delta r}\left(\frac{u_{i+1}^s - u_{i-1}^s + u_{i+1}^{s-1} - u_{i-1}^{-1}}{2}\right)\end{aligned} \tag{26}$$

or in matrix form:

$$A_u U^s = B_u \tag{27}$$

where

$$U^s = \begin{bmatrix} u_1^s \\ u_2^s \\ \vdots \\ u_{N-1}^s \end{bmatrix}, \tag{28}$$

$$A_u = \begin{bmatrix} diag_1 & \frac{-1}{4r_1\Delta r} - \frac{1}{2(\Delta r)^2} & & & \\ \frac{1}{4r_2\Delta r} - \frac{1}{2(\Delta r)^2} & diag_2 & \frac{-1}{4r_2\Delta r} - \frac{1}{2(\Delta r)^2} & & \\ \ddots & \ddots & \ddots & & \\ & & \ddots & \ddots & \\ & & & \frac{1}{4r_{N-1}\Delta r} - \frac{1}{2(\Delta r)^2} & diag_{N-1} \end{bmatrix}, \tag{29}$$

with $diag_i = \left(\frac{\rho}{\mathbb{V}}\frac{1}{\Delta t} + \frac{\rho}{\Gamma(\beta)\mathbb{G}}\frac{a_0}{(\Delta t)^2} + \frac{1}{2(r_i)^2} + \frac{1}{(\Delta r)^2}\right)$, and B_u the column matrix containing all the terms that come from the previous time step.

Equation (24) can also be alternatively written in the matrix form as $A_\sigma \sigma^s = B_\sigma$,

where

$$\sigma^s = \begin{bmatrix} \sigma_1^s \\ \sigma_2^s \\ \vdots \\ \sigma_{N-1}^s \end{bmatrix}, \tag{30}$$

$$A_\sigma = \begin{bmatrix} 1+\frac{\mathbb{V}}{\Gamma(\beta)\mathbb{G}}\frac{b_0}{\Delta t} & & & & \\ & 1+\frac{\mathbb{V}}{\Gamma(\beta)\mathbb{G}}\frac{b_0}{\Delta t} & & & \\ & & \ddots & & \\ & & & \ddots & \\ & & & & 1+\frac{\mathbb{V}}{\Gamma(\beta)\mathbb{G}}\frac{b_0}{\Delta t} \end{bmatrix}, \tag{31}$$

and B_σ is the column matrix containing all the terms that that can be computed with the previous time step values, plus the velocity field variables u_{i+1}^s, u_{i-1}^sthat are already known from solving the velocity equation.

Lemma 3.1. ***(Solvability)*** *Matrices A_u and A_σ are strictly diagonally dominant, and therefore, the discretised velocity and shear stress equations are solvable for each time-step.*

Proof.

For the velocity equation it is sufficient to proove that $\left|\frac{\rho}{\mathbb{V}}\frac{1}{\Delta t}+\frac{\rho}{\Gamma(\beta)\mathbb{G}}\frac{a_0}{(\Delta t)^2}+\frac{1}{2(r_i)^2}+\frac{1}{(\Delta r)^2}\right| > \left|\frac{1}{4r_i\Delta r}-\frac{1}{2(\Delta r)^2}\right|+\left|\frac{-1}{4r_i\Delta r}-\frac{1}{2(\Delta r)^2}\right|$. Let us start by showing that $\left|\frac{1}{2(r_i)^2}+\frac{1}{(\Delta r)^2}\right| > \left|\frac{-1}{4r_i\Delta r}-\frac{1}{2(\Delta r)^2}\right|+\left|\frac{1}{4r_i\Delta r}-\frac{1}{2(\Delta r)^2}\right|$.

$$\begin{aligned} & \left|\tfrac{1}{(r_i)^2}+\tfrac{2}{(\Delta r)^2}\right| > \left|\tfrac{1}{2r_i\Delta r}+\tfrac{1}{(\Delta r)^2}\right|+\left|\tfrac{1}{2r_i\Delta r}-\tfrac{1}{(\Delta r)^2}\right|. \\ \Leftrightarrow\ & \tfrac{1}{(r_i)^2}+\tfrac{1}{(\Delta r)^2} > \tfrac{1}{2r_i\Delta r}+\left|\tfrac{1}{2r_i\Delta r}-\tfrac{1}{(\Delta r)^2}\right| \\ \Leftrightarrow\ & \tfrac{1}{(r_i)^2}+\tfrac{1}{(\Delta r)^2} > \tfrac{1}{2r_i\Delta r}+\left|\tfrac{1}{2r_i\Delta r}-\tfrac{1}{(\Delta r)^2}\right| \\ \Leftrightarrow\ & \tfrac{\Delta r}{r_i}+\tfrac{r_i}{\Delta r} > \tfrac{1}{2}+\left|\tfrac{1}{2}-\tfrac{r_i}{\Delta r}\right| \end{aligned} \tag{32}$$

Since $\frac{r_i}{\Delta r} = \frac{R_i+i\Delta r}{\Delta r} = \frac{R_i}{\Delta r}+i > 1$ for $i = 1, 2, ..., N-1$, we can conclude that A_u is a strictly diagonally dominant matrix. Since a strictly diagonally dominant matrix is nonsingular, we have that for each $s = 1, ..., S$ the inverse matrix A_u^{-1} exists, and therefore equation (27) is solvable.

For the stress equation we just need to note that B_σ is a diagonal matrix, and therefore the stress at each node is obtained directly (assuming the velocity profile is already known).

□

3.2. Numerical Results

In this subsection the convergence of the numerical method will be analysed.

3.2.1. Comparison with Newtonian Fluids

We start by comparing the numerical results obtained for $\beta \to 0$ and $\frac{\mathbb{V}}{\mathbb{G}} \to 0$, with the analytical solution for a Newtonian fluid. We have used the following parameters $\nu = \frac{\mu}{\rho} \equiv \frac{\mathbb{V}}{\rho} = 2 \times 10^{-3}\ m^2.s^{-1}$ (ν, μ are the kinematic and dynamic viscosity, respectively), $\beta = 1 \times 10^{-3}$, $\lambda \equiv \frac{\mathbb{V}}{\mathbb{G}} = 1 \times 10^{-5}\ [s^{1-\beta} \approx s]$, $\Omega_i(t) = c_i t$, $\Omega_o(t) = c_o t$, $c_i = c_o = 1\ s^{-2}$, and boundary conditions $u_\theta(R_{in}, t) = \Omega_i(t) R_{in}$, $u_\theta(R_{out}, t) = \Omega_o(t) R_{out}$ (with R_{in} and R_{out} the inner and outer cylinder radii, respectively). The gap is represented by $h = R_{out} - R_{in}$.

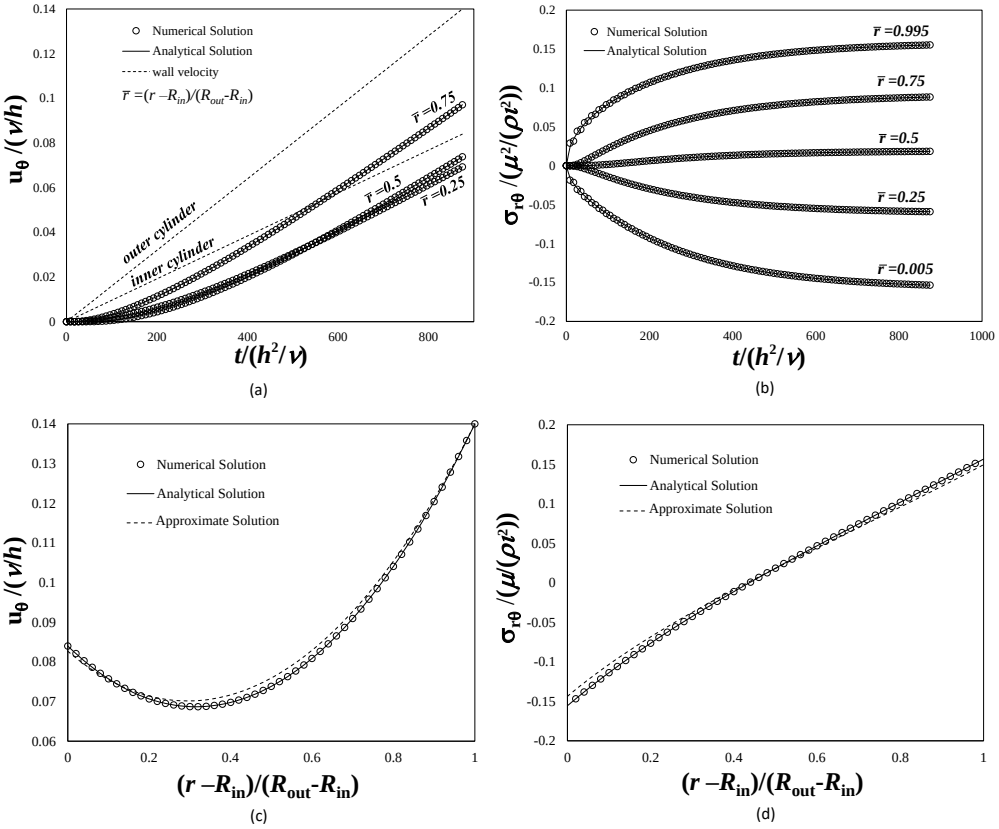

Figure 7: Comparison between analytical, approximate and numerical solutions for the Newtonian annular Couette flow ($\nu = \frac{\mu}{\rho} \equiv \frac{\mathbb{V}}{\rho} = 2 \times 10^{-3}\ m^2.s^{-1}$ (ν, μ are the kinematic and dynamic viscosity, respectively), $\beta = 1 \times 10^{-3}$, $\lambda \equiv \frac{\mathbb{V}}{\mathbb{G}} = 1 \times 10^{-5}\ s^{1-\beta} \approx s$, $\Omega_i(t) = c_i t$, $\Omega_o(t) = c_o t$, $c_i = c_o = 1$, and boundary conditions $u_\theta(R_{in}, t) = \Omega_i(t) R_{in}$, $u_\theta(R_{out}, t) = \Omega_o(t) R_{out}$. The gap is represented by $h = R_{out} - R_{in}$. For the numerical solution we have used $\Delta t/t_c = 3.50 \times 10^{-3}$ (with $t_c = h^2/\nu$) and $\Delta r/h = 5 \times 10^{-3}$) (a),(b) - Variation of velocity and shear stress with time, in different regions; (c),(d) - Velocity and shear stress profiles for $t/t_c = 3.50 \times 10^{-1}$.

The analytical expressions for velocity and shear stress (considering a Newtonian fluid with angular rotation of both the inner and the outer cylinders) are given by [13],

$$\begin{aligned} u_\theta(r,t) &= \frac{c_i R_{in}^2 \left(R_{out}^2 - r^2\right) t + c_o R_{out}^2 \left(r^2 - R_{in}^2\right) t}{r\left(R_{out}^2 - R_{in}^2\right)} - \frac{\pi}{\nu} \sum_{n=1}^{\infty} \frac{J_1(R_{in} r_n) B(r, r_n)}{r_n^2 \left[J_1^2(R_{in} r_n) - J_1^2(R_{out} r_n)\right]} \\ &\quad \times \left(c_o R_{out} J_1(R_{in} r_n) - c_i R_{in} J_1(R_{out} r_n)\right) \left[1 - e^{-\nu r_n^2 t}\right] \end{aligned} \tag{33}$$

$$\begin{aligned}\sigma_{r\theta}(r,t) &= \frac{2\mu R_{in}^2 R_{out}^2 (c_o - c_i)t}{r^2\left(R_{out}^2 - R_{in}^2\right)} - \pi\rho \sum_{n=1}^{\infty} \frac{J_1(R_{in}r_n)\left[2/rB(r,r_n) - r_n\overline{B}(r,r_n)\right]}{r_n^2\left[J_1^2(R_{in}r_n) - J_1^2(R_{out}r_n)\right]} \\ &\times \left(c_o R_{out} J_1(R_{in}r_n) - c_i R_{in} J_1(R_{out}r_n)\right)\left[1 - e^{-\nu r_n^2 t}\right]\end{aligned} \tag{34}$$

where

$$B(r,r_n) = J_1(rr_n)\,\Upsilon_1(R_{out}r_n) - J_1(R_{out}r_n)\,\Upsilon_1(rr_n) \tag{35}$$

$$\overline{B}(r,r_n) = J_0(rr_n)\,\Upsilon_1(R_{out}r_n) - J_1(R_{out}r_n)\,\Upsilon_0(rr_n) \tag{36}$$

r_n (with dimensions m^{-1}) is the n^{th} positive root of the transcendental equation $B(R_{in},r) = 0$, and $J(\cdot)$, $\Upsilon(\cdot)$ are the Bessel functions of first and second kind, respectively. For the numerical solution we have used $\Delta t/t_c = 3.50 \times 10^{-3}$ (with $t_c = h^2/\nu$) and $\Delta r/h = 5 \times 10^{-3}$.

By looking at figures 7(a) and (b), we see the evolution of velocity and stress profiles obtained for $t/t_c = 3.50 \times 10^{-1}$. This is a transient flow, and the numerical method was able to capture accurately the evolution of the different variables. Note that the analytical solution can hardly be distinguished since there is a good agreement between the numerical and the analytical results. As expected we obtain higher velocities for the portion of fluid near the outer cylinder, since this cylinder is rotating at a faster linear velocity (faster than the inner cylinder). The same happens for the stresses. Note that the shear stress is negative near the inner cylinder and positive near the outer cylinder due to the change in sign of the velocity gradient $\partial u_\theta/\partial r$ visible in figure 7(c).

We have also plotted the stress profiles at $t/t_c = 3.50 \times 10^{-1}$. These results are shown in figures 7(b) and (d), and, for this case, three curves are presented. The "numerical solution" is obtained by the numerical method described before; the "approximate solutions" are obtained from equations (33) and (34) using the approximation $r_n \approx n\pi/(R_{out} - R_{in})$, and the "analytical solutions" are obtained again from equations (33) and (34), but now we find the root of the transcendental equation $B(R_{in},r) = 0$ numerically using $n\pi/(R_{out} - R_{in})$ as an initial guess for searching the n^{th} positive root.

From figure 7, it can be concluded that the approximation used, $r_n \approx n\pi/(R_{out} - R_{in})$ [13], reflects on the final result, distorting the correct velocity and stress profiles. We can also conclude that numerical simulation is a viable alternative, that allows the use of realistic boundary conditions (the analytical solution is only available for specific boundary conditions).

3.2.2. Comparison with UCM Numerical Results

In this subsection we will test the applicability of the previously developed numerical method to predict the annular flow of the UCM model - subsection 2.1 (making $\beta \to 0$ in the FVF). For that, we have constructed a simple finite difference code to solve the following system of differential equations governing the unsteady unidirectional flow of a UCM fluid in an annular geometry:

$$\rho\left(\frac{\partial u_\theta}{\partial t} + \lambda\frac{\partial^2 u_\theta}{\partial t^2}\right) = \eta\left(\frac{\partial^2 u_\theta}{\partial r^2} + \frac{1}{r}\frac{\partial u_\theta}{\partial r} - \frac{u_\theta}{r^2}\right) \tag{37}$$

$$\sigma_{r\theta} + \lambda\frac{\partial \sigma_{r\theta}}{\partial t} = \eta\left(\frac{\partial u_\theta}{\partial r} - \frac{u_\theta}{r}\right) \tag{38}$$

$$\sigma_{\theta\theta} + \lambda\frac{\partial \sigma_{\theta\theta}}{\partial t} + \lambda\left\{2\sigma_{r\theta}\left(\frac{u_\theta}{r} - \frac{\partial u_\theta}{\partial r}\right)\right\} = 0 \tag{39}$$

where with $\alpha = 1$, $\beta = 0$ we have $\lambda \equiv \frac{\mathbb{V}}{\mathbb{G}}$, $\eta \equiv \mathbb{V}$.

Note that for the UCM model, the normal stress $\tau_{\theta\theta}$ is not null but is not coupled into the momentum equation (37) (for this specific flow). It can be found subsequently.

Denoting by u_i^s an approximation of $u_\theta\left(R_{in}, t_s\right)$, $\sigma_{r\theta i}^s$ an approximation of $\sigma_{r\theta}\left(R_{in}, t_s\right)$ and $\sigma_{\theta\theta i}^s$ an approximation of $\sigma_{\theta\theta}\left(R_{in}, t_s\right)$ the discretised system of equations is given by:

$$\rho\left(\frac{u_i^s - u_i^{s-1}}{\Delta t} + \lambda\frac{u_i^s - 2u_{i-1}^{s-1} + u_{i-2}^{s-1}}{\Delta t^2}\right) = \eta\left(\frac{u_{i-1}^s - 2u_i^s + u_{i+1}^s}{\left(\Delta r\right)^2} + \frac{u_{i+1}^s - u_{i-1}^s}{2R_{in}\Delta r} - \frac{u_i^s}{R_{in}}\right) \tag{40}$$

$$\sigma_{r\theta i}^s + \lambda\frac{\sigma_{r\theta i}^s - \sigma_{r\theta i}^{s-1}}{\Delta t} = \eta\left(\frac{u_{i+1}^s - u_{i-1}^s}{2\Delta r} - \frac{u_i^s}{R_{in}}\right) \tag{41}$$

$$\sigma_{\theta\theta i}^s + \lambda\frac{\sigma_{\theta\theta i}^s - \sigma_{\theta\theta i}^{s-1}}{\Delta t} + \lambda\left\{2\sigma_{r\theta i}^s\left(\frac{u_i^s}{R_{in}} - \frac{u_{i+1}^s - u_{i-1}^s}{2\Delta r}\right)\right\} = 0 \tag{42}$$

The approximations used for each term are obvious. The equations are solved sequentially and, based on the discretisation employed for each term, we expect a convergence order of 1 in time and 2 in space.

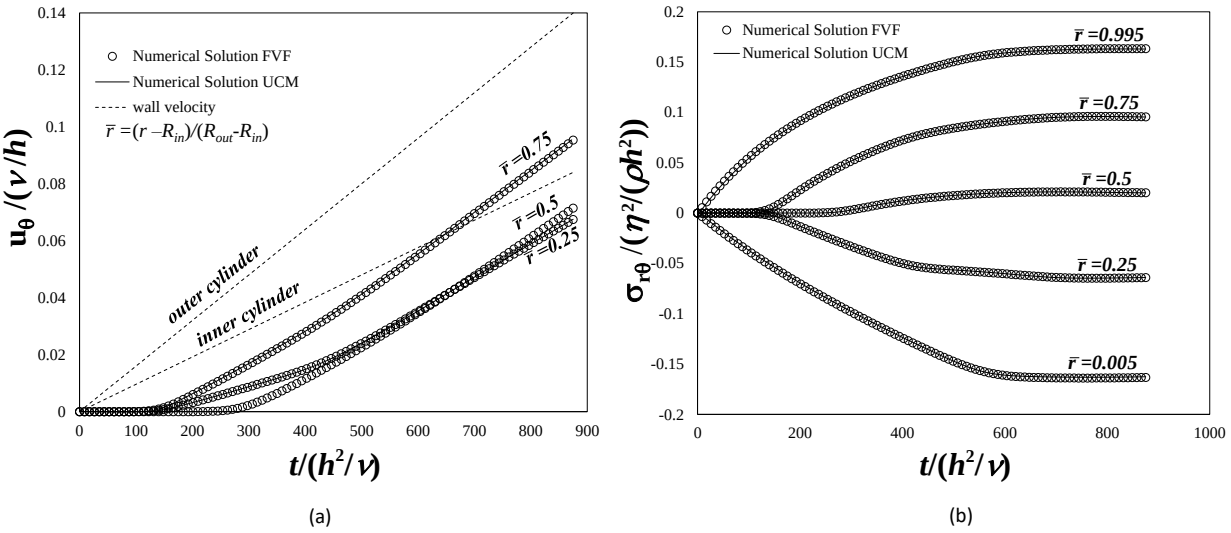

Figure 8: Comparison between the numerical codes developed for the FVF and UCM annular flows ($\nu = \frac{\eta}{\rho} \equiv \frac{\mathbb{V}}{\rho} = 1 \times 10^{-3}\ m^2 s^{-1}$ (ν, η are the kinematic and dynamic viscosity, respectively), $\beta = 1 \times 10^{-6}$, $El = \frac{\lambda}{t_v} = 6.25 \times 10^{-2}$ with $t_v = \frac{h^2}{\nu}$, $\Omega_i(t) = c_i t$, $\Omega_o(t) = c_o t$, $c_i = c_o = 1$, and boundary conditions $u_\theta(R_{in}, t) = \Omega_i(t) R_{in}$, $u_\theta(R_{out}, t) = \Omega_o(t) R_{out}$. For the FVF code we have used $\Delta t/t_v = 3.5 \times 10^{-3}$ and $\Delta r/h = 5 \times 10^{-3}$, and for the UCM code $\Delta t/t_v = 1 \times 10^{-3}$ and $\Delta r/h = 2 \times 10^{-3}$) (a)-Velocity profile; (b)-shear stress profile.

As an example of validation we have compared the velocity and shear stress profiles obtained with both numerical methods (fractional and classical). We used the same parameters as in the Newtonian case, except now $\beta = 1 \times 10^{-6}$. For the viscoelastic fluid we have also considered an elasticity number, $El = \frac{\lambda}{t_v} = 6.25 \times 10^{-2}$ with $t_v = \frac{h^2}{\nu}$. In the Newtonian case we have $El = 0$.

The mesh resolution used in the FVF simulations was $\Delta t/t_v = 3.5 \times 10^{-3}$ and $\Delta r/h = 5 \times 10^{-3}$, and for the UCM code$\Delta t/t_v = 1 \times 10^{-3}$ and $\Delta r/h = 2 \times 10^{-3}$.

Figure 8 shows the evolution in time of the angular velocity and shear stress at different positions across the gap between the cylinders. Since in this case the relaxation time of the viscoelastic fluid plays an important role it is expected that there will be slower momentum transfer from the walls to the bulk of the fluid (when compared to the Newtonian case), as shown by comparing figures 8(a) and 7 (a). Note that for $\overline{r} = 0.5$ the fluid responds most slowly, since this region is most far removed from both rotating cylinders. The variation of the shear stress with time is also more smooth when compared to the Newtonian case, especially when the outer cylinder starts rotating. This is again due to the fast purely diffusive propagation of information from the wall to the fluid, in the Newtonian case.

The results obtained with the different codes are perfectly superimposed. We have tested the UCM code considering different levels of mesh refinement (doubling the number of cells in t and r, for each successive mesh). For the most refined mesh and the mesh used in the simulations the differences were visually indistinguishable.

3.2.3. Experimental Order of Convergence

To further verify the numerical code and determine the order of convergence of the proposed method we have *created* two distinct analytical solutions, by imposing a certain velocity or stress profile, through the inclusion of correcting source terms, $f(t,r)$ (the source terms force the solution to be verified by the equation). This is known as the method of manufactured solutions [77, 78]. First we only verify the discretised velocity equation, that is independent of the stress, and then we verify the discretised stress equation, which depends on the computed velocity profile and its spatial derivative.

Momentum Equation for the Tangential Velocity

For the evolution in the discretised tangential velocity we have considered the following problem with $R_{in} = 1\ m$, $R_{out} = 2\ m$ and $\beta = 0.5$ (we have also considered $\nu = \frac{\mathbb{V}}{\rho} = 1\ m^2.s^{-1}$, $\mathbb{V} = 1\ Pa.s^{\alpha}$, $\mathbb{G} = 1\ Pa.s^{\beta}$, $\Delta r \in [1/4,\ 1/32]m$ and $\Delta t \in [1/8,\ 1/256]s$):

$$\frac{\partial u_\theta}{\partial t} + D_t^{2-\beta}\left(u_\theta\right) = \frac{\partial^2 u_\theta}{\partial r^2} + \frac{1}{r}\frac{\partial u_\theta}{\partial r} - \frac{u_\theta}{r^2} + f\left(t,r\right) \tag{43}$$

$$\begin{aligned} f\left(r,t\right) = \ & \tfrac{3r^3(10r-3)t^{2-\alpha}}{5\Gamma(3-\alpha)} + 3r^3\left(r-\tfrac{3}{10}\right)t^2 - \left(6r^2+6\left(r-\tfrac{3}{10}\right)r\right)t^3 \\ & -\tfrac{r^3t^3+3r^2\left(r-\frac{3}{10}\right)t^3}{r} + r\left(r-\tfrac{3}{10}\right)t^3 \end{aligned} \tag{44}$$

with boundary and initial conditions:

$$u_\theta\left(R_{in},t\right) = t^3R_{in}^3(R_{in}-\frac{3}{10}),\ u_\theta\left(R_{in},t\right) = t^3R_{out}^3(R_{out}-\frac{3}{10}),\ \ 0<t<T \tag{45}$$

$$u_\theta\left(r,0\right) = 0,\ \frac{\partial u_\theta\left(r,0\right)}{\partial t} = 0,\ \ R_{in} < r < R_{out} \tag{46}$$

whose analytical solution is given by,

$$u_\theta\left(r,t\right) = t^3r^3(r-\frac{3}{10}). \tag{47}$$

The following expression will be used, to evaluate the accuracy of the numerical predictions,

$$\varepsilon_{\Delta r,\Delta t} = \max_{k=1,...,N-1} \left| u_\theta \left(R_{in} + r_k, t_i \right) - u_\theta^{num} \left(R_{in} + r_k, t_i \right) \right|, \ i = 1, 2, ..., S \tag{48}$$

with the convergence order, which is given by,

$$p_u = \log \left(\frac{\varepsilon_{\Delta r,\Delta t}}{\varepsilon_{\Delta r/2,\Delta t}} \right) / \log \left(2 \right) \tag{49}$$

for space and

$$q_u = \log \left(\frac{\varepsilon_{\Delta r,\Delta t}}{\varepsilon_{\Delta r,\Delta t/2}} \right) / \log \left(2 \right) \tag{50}$$

for time, with $r_k = k\Delta r$ and $t_i = i\Delta t$. Here $u_\theta^{num} \left(R_{in} + r_k, t_i \right)$ stands for the numerical solution obtained at $R_{in} + r_k$ (instant t_i).

An excellent agreement between the analytical and numerical solutions was obtained, resulting in a convergence order of ≈ 1 in time and ≈ 2 in space (see Tables 1 and 2).

Table 1: Error norms and rates of convergence (at $t = 1$).

Δt	Δr	$\varepsilon_{\Delta r,\Delta t}$	p_u
1/1000	1/4	0.020330	-
1/1000	1/8	0.005018	2.02
1/1000	1/16	0.001102	2.19
1/1000	1/32	0.000190	2.53

Table 2: Error norms and rates of convergence (at $t = 1$).

Δt	Δr	$\varepsilon_{\Delta r,\Delta t}$	q_u
1/8	1/2500	0.028452	-
1/16	1/2500	0.011964	1.25
1/32	1/2500	0.007381	0.70
1/64	1/2500	0.004201	0.81
1/128	1/2500	0.002284	0.88
1/256	1/2500	0.001208	0.92

Constitutive Equation for the Tangential Stress

For the discretised stress equation we assume $R_{in} = 1\ m$, $R_{out} = 2\ m$ and $\beta = 0.5$ (we have also considered $\mathbb{V} = 1\ Pa.s^\alpha$, $\mathbb{G} = 1\ Pa.s^\beta$, $\Delta r = 1/500\ m$ and $\Delta t \in [1/8,\ 1/128]s$) and we impose a stress profile given by,

$$\sigma_{r\theta} \left(r, t \right) = r^2 t^3 \tag{51}$$

The substitution of this stress profile into equation (13) results in the following differential equation to be solved analytically,

$$\frac{\partial u_\theta \left(r, t \right)}{\partial r} - \frac{u_\theta \left(r, t \right)}{r} = r^2 t^3 \left(\frac{6t^{-(1-\beta)}}{\Gamma(4-(1-\beta))} + 1 \right). \tag{52}$$

Table 3: Error norms and convergence rates (at $t = 1$).

Δt	Δr	$\varepsilon^{\sigma}_{\Delta r,\Delta t}$	q_σ
1/8	1/500	0.091197	-
1/16	1/500	0.034317	1.41
1/32	1/500	0.012637	1.44
1/64	1/500	0.004591	1.46
1/128	1/500	0.001653	1.47

For the solution of this differential equation we choose the boundary condition $u_\theta(1,t) = 0$ (the boundary condition is not important here), resulting in the following velocity profile,

$$u_\theta(r,t) = \frac{r\left(r^2-1\right)t^{3-(1-\beta)}\left(\Gamma(4-(1-\beta))t^{(1-\beta)}+6\right)}{2\Gamma(4-(1-\beta))} \tag{53}$$

The discretised stress equation was then numerically solved using the derived exact velocity profile (see equation (24)):

$$\sigma_i^s \quad + \frac{1}{\Gamma(\beta)}\frac{1}{\Delta t}\left[b_0\sigma_i^s - \sum_{j=0}^{s-1}\left(b_{n-j-1}-b_{n-j}\right)\sigma_i^j\right] = \frac{\partial u_\theta(r,t)}{\partial r} - \frac{u_\theta(r,t)}{r} \tag{54}$$

with coefficients b_l given by Eq. (25).

This way we can measure the error committed in the approximation of

$$\sigma_{r\theta} + D_t^{1-\beta}\sigma_{r\theta} \tag{55}$$

by

$$\sigma_i^s + \frac{1}{\Gamma(\beta)}\frac{1}{\Delta t}\left[b_0\sigma_i^s - \sum_{j=0}^{s-1}\left(b_{n-j-1}-b_{n-j}\right)\sigma_i^j\right]. \tag{56}$$

The convergence order is given by,

$$q_\sigma = \log\left(\frac{\varepsilon^{\sigma}_{\Delta r,\Delta t}}{\varepsilon^{\sigma}_{\Delta r,\Delta t/2}}\right)/\log(2) \tag{57}$$

with

$$\varepsilon^{\sigma}_{\Delta r,\Delta t} = \max_{k=1,\ldots,N-1}\left|\sigma_\theta\left(R_{in}+r_k,t_i\right) - \sigma_\theta^{num}\left(R_{in}+r_k,t_i\right)\right|,\ i = 1,2,...,S \tag{58}$$

where $\sigma_\theta^{num}\left(R_{in}+r_k,t_i\right)$ stands for the numerical solution obtained at $\left(R_{in}+r_k,t_i\right)$ (instant t_i).

By looking at Table (3) we see that the convergence order for the stress is $q_\sigma \approx 1.4$. This order is expected to decrease when the complete system of equations is solved, and the velocity profile is not exact.

4. Results

4.1. Stress Relaxation

In order to test the influence of the order of the derivative on the evolution in the stress field, we have have simulated a typical stress relaxation experiment in an annular geometry. We impose

a *step strain*, i.e. the outer cylinder suddenly starts rotating and then stops (after a period of $\Delta t_{exp} \approx 50\ ms$). Then we observe how the tangential stress in the fluid relaxes.

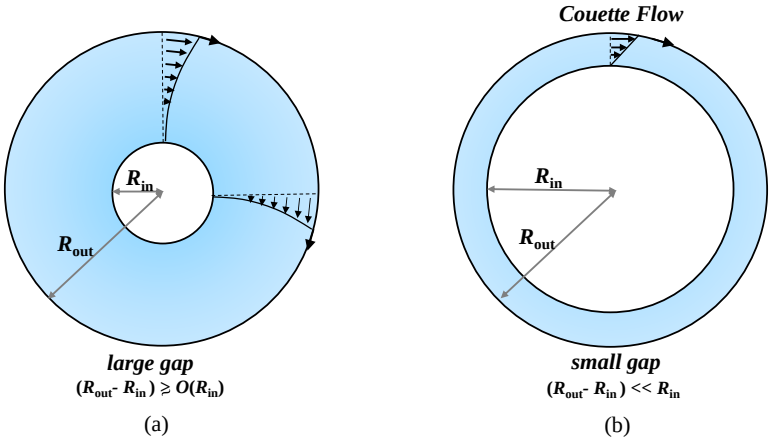

Figure 9: Influence of the gap on the type of flow. (a) $\frac{h}{R_{in}} \sim O(1)$; (b) $\frac{h}{R_{in}} \ll 1$.

We consider an annulus of fluid confined between two cylinders of radii $R_{in} = 22.65\,mm$ and $R_{out} = 25\,mm$, leading to a gap of $h = 2.35\,mm$ [44]. Before showing any results on the evolution of velocity and stress, it should be recalled that when the gap between the two cylinders is small compared to the inner radius, $(R_{out} - R_{in}) \ll R_{in}$ (see figure 9) we approach a simple Couette flow. In this case we have that $\frac{h}{R_{in}} = \frac{R_{out} - R_{in}}{R_{in}} \approx 0.1$ meaning that the gap between the two cylinders is much smaller than the radius of the inner cylinder. For this simulation we have considered the model parameters obtained for the xanthan gum with a concentration of 0.25 $wt.\%$, that is, $\mathbb{V} = 24.96\ Pa.s$, $\mathbb{G} = 1.56\ Pa.s^{\beta}$, $\beta = 0.31$ and $\tau = 55.6\ s$.

The outer cylinder starts rotating at $t = 0^+$ with a tangential velocity given by, $u_\theta\left(R_{out}, t\right) = \dot{\theta}(t) R_{out}$, where

$$\dot{\theta}\left(t\right) = \frac{\Delta\theta}{\psi\sqrt{\pi}} e^{-\frac{(t-t_d)^2}{\psi^2}}. \tag{59}$$

Note that as $\psi \to 0$, the velocity $u_\theta\left(R_{out}, t\right)$ converges to the Dirac delta function multiplied by the angle turned, $\Delta\theta\delta(t)$ [79] (assuming $t_d = 0$). The need for the delay time, t_d, comes from the initial condition $\frac{du_\theta(R_{out},0)}{dt} = 0$ and from the fact that $\frac{du_\theta(R_{out},t)}{dt} \to 0$ as $|t| \to \infty$. The mesh size used in the simulations is $\Delta t/\tau = 1.79856 \times 10^{-5}$, $\Delta r/h = 1 \times 10^{-2}$, and we have considered three different straining deformations ($\gamma_0 = \Delta\theta R_{out}/h$) of 1%, 5% and 100%. After a time of ≈ 50 ms ($t/\tau \sim 0.0009$) the outer cylinder has already rotated from A to B (clockwise), and stopped (see figure 10). Note that the position of B varies with the imposed deformation.

During this sudden straining motion we measure the evolution of the shear stress at a particular point, $(\overline{r} = (r - R_{in})/(R_{out} - R_{in}) = 0.25)$. Note that in the narrow gap limit $h/R_{in} \ll 1$ there is an analytical solution for the problem under study, given by [51, 80],

$$\frac{\sigma(t)}{\gamma_0} = \mathbb{G}(t - t_d)^{-\beta} E_{1-\beta,1-\beta}\left(-\frac{\mathbb{G}}{\mathbb{V}}(t - t_d)^{1-\beta}\right) \tag{60}$$

where $E_{1-\beta,1-\beta}$ is the generalized Mittag-Leffler function [4]. It should also be remarked that we

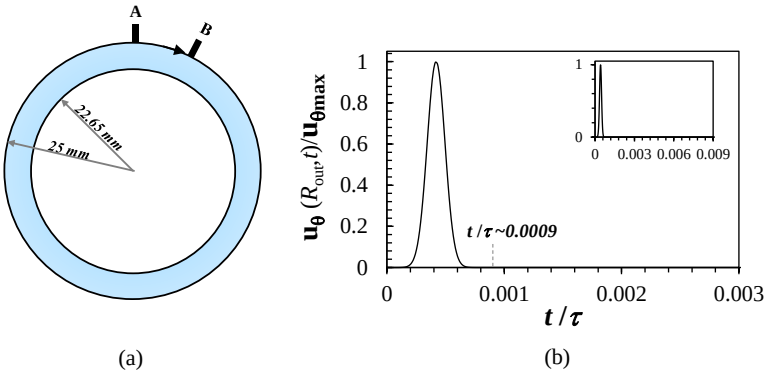

Figure 10: Stress relaxation test in a narrow gap cylindrical Couette cell following a sudden straining deformation (the outer cylinder rotates from A to B in a time $t/\tau \approx 9 \times 10^{-4}$ and then stops) (a) Annular geometry and dimensions; (b) Normalised tangential velocity ($u_{\theta max} = u_\theta\,(R_{out}, t_d)$) of the outer cylinder (case of $\gamma_0 = 100\%$). The normnalized delay time is $t_d/\tau = 4.5 \times 10^{-4}$.

have shifted the analytical solution by t_d in time due to the delay used in the numerical solution (needed to ensure that $du_\theta/dt \to 0$ at $t = 0$).

We first show (figure 11(a)) the normalised shear stress relaxation results obtained for a step-strain test with a deformation of $\gamma_0 = 100\%$, $\beta = 0.31$ and three different levels of refinement, $\psi/\tau = 1.0 \times 10^{-4}$, 1.8×10^{-4}, 2.7×10^{-4} and a normalized delay time of $t_d/\tau = 4.5 \times 10^{-4}$, 7.4×10^{-4}, 1.1×10^{-3}. Note that as $\psi \to 0$ the outer cylinder has to rotate faster to attain the same fixed *distance turned* in a progressively shorter period of time. This makes the numerical calculation increasingly stiff, since we have to capture accurately high gradients.

Convergence to the analytical solution is observed as we decrease the value of ψ.

The evolution of the deformation in time for the three different tangential velocities imposed on the outer cylinder is shown in figure 11(b). As expected, with progressive increases of the rotation velocity, a sharper approximation of a true step-strain displacement is obtained.

The normalised stress relaxation for the three different levels of imposed deformations are shown in figures 11(c) and (d). The results were compared with the analytical solution, and a good match between analytical and numerical solutions was obtained for the different imposed deformations. This supports our claims that the numerical code is robust and can be used in the prediction of real fluid behavior, modeled by the FVF.

The true power of the fractional model can be seen for the case where different fractional exponents are considered, as shown in figure 12 for a deformation of $\gamma_0 = 100\%$, $\psi/\tau = 7.4 \times 10^{-5}$, $t_d/\tau = 6.2 \times 10^{-4}$, and $\beta = 0.1, 0.25, 0.5$. Due to large simulation times we have also modified the numerical code to deal with graded meshes in time.

After some numerical experiments we observed that a good mesh grading could be given by:

$$t_s = \begin{cases} 2t_d - 2t_d\left(1 - \frac{s}{N_1}\right)^{r_1} & s < N_1 \\ 2t_d - 2T\left(\frac{s-N_1}{N_2}\right)^{r_2} & s \geqslant N_1 \end{cases} \tag{61}$$

where T is the duration of the experiment, $N_1 = 50$, $N_2 = 1000$, $r_1 = 1$, $r_2 = 1.693$. With this graded mesh we managed to obtain a speed up of up to $\approx 55\times$, allowing us to perform simulations of $\frac{\Delta t_{exp}}{\tau} \approx 2.2$ in a feasible computational time (the numerical simulations were performed with the

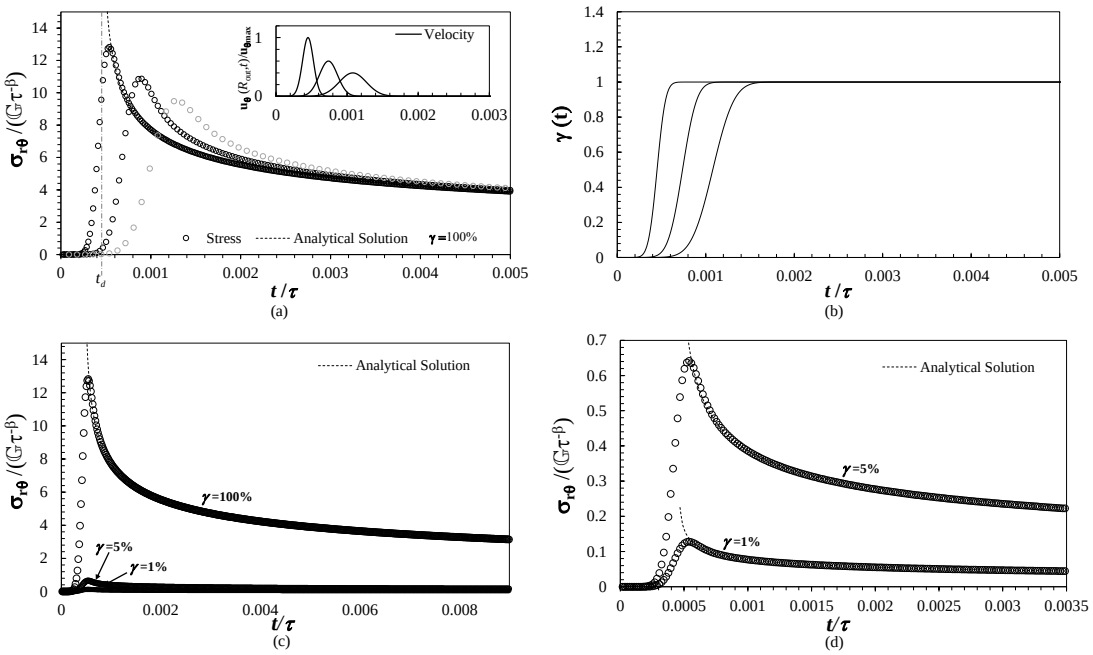

Figure 11: (a) Normalised shear stress relaxation obtained for a step-strain test with a deformation of $\gamma_0 = 100\%$, $\beta = 0.31$ and three different levels of refinement, $\psi/\tau = 1.0 \times 10^{-4}$ ($t_d/\tau = 4.5 \times 10^{-4}$), $\psi/\tau = 1.8 \times 10^{-4}$ ($t_d/\tau = 7.4 \times 10^{-4}$) and $\psi/\tau = 2.7 \times 10^{-4}$ ($t_d/\tau = 1.1 \times 10^{-3}$). A comparison with the analytical solution (equation (60)) is also performed (inset: imposed outer cylinder velocity for the three values of ψ/τ and t_d/τ from Eq. (59). The normalisation was performed with the maximum velocity obtained for $\psi/\tau = 1.0 \times 10^{-4}$). (b) Evolution of the deformation ($\gamma(t) = \Delta\theta R_{out}/h$) in time for the three different tangential velocities imposed. (c) Stress relaxation for three different deformations 1%, 5% and 100% ($\psi/\tau = 1.0 \times 10^{-4}$ and $t_d/\tau = 4.5 \times 10^{-4}$). (d) Zoomed view of the stress relation obtained for the two smaller deformations. In the simulations we have considered $\Delta t/\tau = 1.79856 \times 10^{-5}$, $\Delta r/h = 1 \times 10^{-2}$.

software Mathematica (V. 11) in a computer with a processor Intel(R) Core(TM)i7-4650U CPU @ 1.70GHz 2.30GHz and 8Gb of RAM).

Figure 12 shows the relaxation of the normalised stress on a logarithmic scale and an inset on a linear scale. It is well known [4] that for $t \ll \tau$ the asymptotic limits of the stress relaxation function for the Fractional Maxwell Model are given by $G(t) \approx \mathbb{G}t^{-\beta}/\Gamma(1-\beta)$ and by $G(t) \approx \mathbb{V}t^{-\alpha}/\Gamma(1-\alpha)$ for $t \gg \tau$. Therefore we have that for $t \ll \tau$:

$$\log\left(\frac{\sigma(t)}{\mathbb{G}\tau^{-\beta}}\right) = \log\left(\frac{\gamma_0}{\Gamma(1-\beta)}\right) - \beta\ \log\left(\frac{t}{\tau}\right). \tag{62}$$

This equation is represented in figure 12 by dashed lines.

By looking at figure 12 (including the inset) we see that for small values of β the springpot converges to a spring, leading to an approximate Maxwell behaviour, that is obtained when $\alpha \to 1$ and $\beta \to 0$ ($\sigma(t) + \frac{\mathbb{V}}{\mathbb{G}}\frac{d\sigma(t)}{dt} = \mathbb{V}\dot{\gamma}(t)$), and therefore, the peak of the stress is smaller, but, it takes more time to relax (smaller rate of relaxation). As we increase the value of β, the FVF evolves towards a Newtonian fluid, since each springpot converges to a dashpot when $\alpha \to 1$ and $\beta \to 1$ ($\sigma(t) = \frac{\mathbb{V}\mathbb{G}}{\mathbb{V}+\mathbb{G}}\dot{\gamma}(t)$), thus increasing the relaxation rate.

Finally, we study the stress relaxation of the FMM upon a sudden deformation (see figure 10).

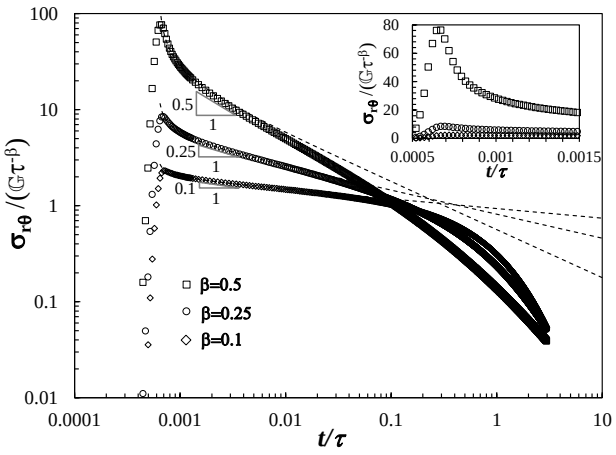

Figure 12: Normalised shear stress relaxation obtained for the step-strain test shown in figure 10 considering the FVF, $\gamma_0 = 100\%$, $\psi/\tau = 7.4 \times 10^{-5}$, $t_d/\tau = 6.2 \times 10^{-4}$, and $\beta = 0.1, 0.25, 0.5$ ($\mathbb{G}$ was kept constant, and, $\mathbb{V}$ varied with β so that τ could be the same for the different β values). In the simulations we have considered $\Delta t_{min}/\tau = 2.48 \times 10^{-5}$, $\Delta r/h = 1 \times 10^{-2}$. The dashed lines represent the analytical asymptotic values expected. The inset shows a zoomed view of the high gradients region.

In order to realize this response, at each time step we have to take into account all the deformation history from t_0 (beginning of the experiment) to t_s (actual time). The computational method becomes more expensive, and therefore, the use of a graded mesh [81, 82, 83, 84] in time allows a huge reduction in simulation time, especially for this case where the gradients of velocity and stress drastically reduce after the jump in deformation. For more details please see Appendix B.

Figure 13 shows the relaxation of the normalised shear stress on logarithmic axes (and the inset shows the normalised stress relaxation on linear axes) for $\gamma_0 = 100\%$, $\psi/\tau = 7.4 \times 10^{-5}$, $t_d/\tau = 6.2 \times 10^{-4}$, $\beta = 0.25$ and two different values of α (0.5,0.7). We also show the asymptotic values obtained for small and large times. For $t \gg \tau$ we have that [4]:

$$\log\left(\frac{\sigma(t)}{\mathbb{G}\tau^{-\beta}}\right) = \log\left(\frac{\gamma_0}{\Gamma(1-\alpha)}\right) - \alpha\ \log\left(\frac{t}{\tau}\right), \tag{63}$$

(for $t \ll \tau$ see Eq. (63)) and therefore in figure 13 we can observe two distinct relaxation processes, shown by the different slopes of the dashed lines for $t \ll \tau$ and $t \gg \tau$.

For this case study we kept $\mathbb{G}$ constant and $\mathbb{V}$ varied with α so that τ could be the same for the different α values. Since β is low, it is interesting to see the differences in the long time relaxation dynamics for the two different values of α used. When α is low, we obtain in the dual limit $(\alpha - \beta) \to 0$ and $\alpha \to 0$ an equation for an elastic solid ($\sigma(t) = \frac{\mathbb{V}\mathbb{G}}{\mathbb{V}+\mathbb{G}}\gamma(t)$), meaning that the rate of relaxation will be slower in this limit (see figure 13). When β is low and α is high, we obtain, in the limit $(\alpha - \beta) \to 1$ and $\alpha \to 1$, the Maxwell model. As α increases we see an increase in relaxation rate as per Eq. 63.

Note that for the same simulation time, it is more difficult to approach the asymptotic values expected for $t \ll \tau$ and $t \gg \tau$, when α is low. Therefore we have also plotted the analytical solution (full line in figure 13)) for the case $\alpha = 0.5$. This analytical solution is a generalisation of equation (60), [51, 80], being given by:

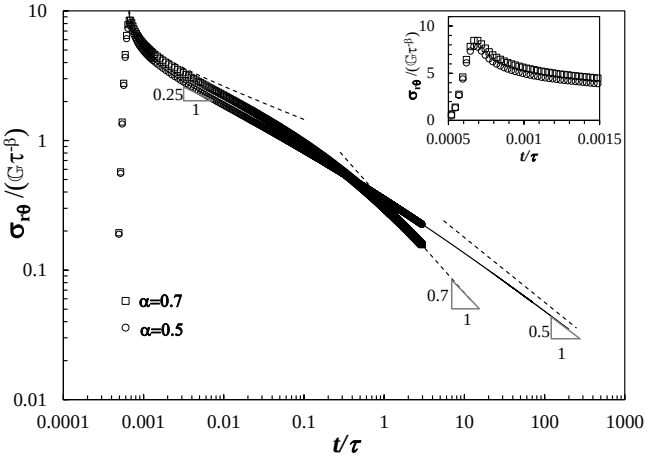

Figure 13: Normalised shear stress relaxation obtained for the step-strain test shown in figure 10 considering the FMM, $\gamma_0 = 100\%$, $\psi/\tau = 7.4 \times 10^{-5}$, $t_d/\tau = 6.2 \times 10^{-4}$, $\beta = 0.25$ and $\alpha = 0.5, 0.7$. Here $\mathbb{G}$ was kept constant and $\mathbb{V}$ varied with α so that τ could be the same for the different α values. In the simulations we have considered $\Delta t_{min}/\tau = 2.48 \times 10^{-5}$, $\Delta r/h = 1 \times 10^{-2}$.

$$\frac{\sigma(t)}{\gamma_0} = \mathbb{G}(t - t_d)^{-\beta} E_{\alpha-\beta,1-\beta}\left(-\frac{\mathbb{G}}{\mathbb{V}}(t - t_d)^{\alpha-\beta}\right). \tag{64}$$

We see again that the results obtained with the numerical method match the analytical solution, proving the robustness of the numerical code and its ability to solve both fast initial transients and long time asymptotic relaxation dynamics.

5. Discussion and Conclusions

A numerical method for the solution of the coupled system of equations arising in the pure tangential annular flow of fractional viscoelastic fluids was presented. The method can resolve fast transients and stress relaxations following step strains. We studied the convergence order using numerical experiments and proved its solvability. The stability and theoretical convergence of the method will be presented in the future.

A discussion of the admissibility of certain fractional viscoelastic models proposed in the literature was presented, and we have distinguished two types of models, the four parameter FMM that allows a better fit of experimental data but that shows unbounded stress growth following start up of steady shear, and the three parameter FVF model that also allows a good fit of experimental data and that shows bounded stress growth following start up of steady shear, this therefore being an ideal model for fluids.

The numerical method used in the solution of the FMM is slightly different from the one used in the FVF, since the past deformation needs to be taken into account at each time-step. This led to an increase in simulation time, and therefore, graded meshes were used for the discretisation in time.

The results presented in this work for the FVF and FMM show that these models are a promising tool for modeling the transient response of realistic complex fluids. However, it is important to note that neither model can capture the shear thinning observed at large strains and high

Weissenberg numbers [26]. To describe these nonlinear effects it will be important in future work to also incorporate nonlinear effects in the integral expressions for the stress, for example through a factorizable equation of K-KBKZ form [26, 85, 42].

Acknowledgements

L.L. Ferrás and J.M. Nóbrega would like to thank the funding by FEDER through the COMPETE 2020 Programme, the National Funds through FCT - Portuguese Foundation for Science and Technology under the project UID/CTM/50025/2013. L.L. Ferrás would also like to thank the funding by FCT through the scholarship SFRH/BPD/100353/2014. M.L. Morgado would like to thank the funding by FCT through Project UID/MAT/00013/2013 and M. Rebelo would also like to thank the funding by FCT through Project UID/MAT/00297/2013 (Centro de Matemática e Aplicações).

References

[1] M.R. Brown, D.J. Curtis, P. Rees, H.D. Summers, K. Hawkins, P.A. Evans, P.R. Williams, Fractal discrimination of random fractal aggregates and its application in biomarker analysis for blood coagulation. Chaos, Solitons & Fractals 45 (2012) 1025-1032.

[2] C.E. Wagner, A.C. Barbati, J. Engmann, A.S. Burbidge, G.H. McKinley, Quantifying the consistency and rheology of liquid foods using fractional calculus, Food Hydrocolloids 69 (2017) 242-254.

[3] R.G. Owens, T.N. Phillips, Computational rheology. Vol. 14. London: Imperial College Press, 2002.

[4] I. Podlubny, Fractional differential equations: an introduction to fractional derivatives, fractional differential equations, to methods of their solution and some of their applications. Vol. 198. Academic press, 1998.

[5] F. Mainardi, Fractional calculus and waves in linear viscoelasticity: an introduction to mathematical models. World Scientific, 2010.

[6] A. Jaishankar, G.H. McKinley, Power-law rheology in the bulk and at the interface: quasi-properties and fractional constitutive equations, Proc. R. Soc. A. The Royal Society, (2012) DOI: 10.1098/rspa.2012.0284.

[7] A.N. Beris, R.C. Armstrong, R.A. Brown, Perturbation theory for viscoelastic fluids between eccentric rotating cylinders, J. Non-Newt. Fluid Mech. 13 (1983) 109143.

[8] R.K. Bhatnagar, Steady laminar flow of visco-elastic fluid through a pipe and through an annulus with suction or injection at the walls, J. Ind. Inst. Sci. 45 (1963) 126151.

[9] R.B. Bird, R.C. Armstrong, O. Hassager, Dynamics of Polymeric Liquids. Fluid Mechanics, second ed., vol. I. Wiley, 1987.

[10] D.O.A. Cruz, F.T. Pinho, Skewed Poisueille-Couette flows of SPTT fluids in concentric annuli and channels, J. Non-Newt. Fluid Mech. 121 (2004) 1-14.

[11] A.C. Dierckes, W.R. Schowalter, Helical flow of a non-Newtonian polyisobutelene solution, Ind. Eng. Chem. Fund. 5 (1966) 263 271.

[12] M. Athar, C. Fetecau, M. Kamran, A. Sohail, M. Imran, Exact solutions for unsteady axial Couette flow of a fractional Maxwell fluid due to an accelerated shear, Modelling and Control 16 (2011) 135151.

[13] M. Imran, A.U. Awan, M. Rana, M. Athar, M. Kamran, Exact Solutions for the Axial Couette Flow of a Fractional Maxwell Fluid in an Annulus, ISRN Mathematical Physics 2012 (2012) 1-15.

[14] K. Khandelwal, V. Mathur, Exact solutions for an Unsteady Flow of Viscoelastic Fluid in Cylindrical Domains Using the Fractional Maxwell Model, Int. J. Appl. Comput. Math. 1 (2015) 143-146.

[15] A. Mahmood, S. Parveen, A. Ara, N.A. Khan, Exact analytic solutions for the unsteady flow of a non-Newtonian fluid between two cylinders with fractional derivative model, Commun Nonlinear Sci Numer Simulat 14 (2009) 33093319.

[16] H. Qi, H. Jin, Unsteady rotating flows of a viscoelastic fluid with the fractional Maxwell model between coaxial cylinders, Acta Mechanica Sinica 22 (2006) 301-305.
[17] W. Shaowei, X. Mingyu, Axial Couette flow of two kinds of fractional viscoelastic fluids in an annulus, Nonlinear Analysis: Real World Applications 10 (2009) 1087-1096.
[18] M. Jamil, N.A. Khan, A.A. Zafar, Translational flows of an Oldroyd-B fluid with fractional derivatives, Computers and Mathematics with Applications 62 (2011) 15401553.
[19] K. Khandelwal, V. Mathur, Unsteady unidirectional flow of Oldroyd-B fluid between two infinitely long coaxial cylinders, Int Jr. of Mathematical Sciences & Applications 4 (2014) 1-10.
[20] Y. Liu, , F. Zong, J. Dai, Unsteady Helical Flow of a Generalized Oldroyd-B Fluid with Fractional Derivative, International Journal of Mathematics Trends and Technology 5 (2014) 67-77.
[21] A. Mahmood, On analytical study of fractional Oldroyd-B flow in annular region of two torsionally oscillating cylinders, Thermal Science 16 (2012) 411-421.
[22] V. Mathur, K. Khandelwal, Exact solution for the flow of Oldroyd-B fluid due to constant shear and time dependent velocity, Journal of Mathematics 10 (2014) 38-45.
[23] D. Tong, Y. Liu, Exact solutions for the unsteady rotational flow of non-Newtonian fluid in an annular pipe, International Journal of Engineering Science 43 (2005) 281289.
[24] D. Tong, X. Zhang, X. Zhang, Unsteady helical flows of a generalized Oldroyd-B fluid, J. Non-Newtonian Fluid Mech. 156 (2009) 7583.
[25] L.I. Palade, P. Attane, R.R. Huilgol, B. Mena, Anomalous stability behavior of a properly invariant constitutive equation which generalises fractional derivative models, International journal of engineering science 37 (1999) 315-329.
[26] A. Jaishankar, G.H. McKinley, A fractional K-BKZ constitutive formulation for describing the nonlinear rheology of multiscale complex fluids, Journal of Rheology 58 (2014) 1751-1788.
[27] Z.Z. Sun, X. Wu, A fully discrete difference scheme for a diffusion-wave system, Applied Numerical Mathematics 56 (2006) 193-209.
[28] k. Diethelm, N.J. Ford, A.D. Freed, A predictor-corrector approach for the numerical solution of fractional differential equations, Nonlinear Dynamics 29 (2002) 3-22.
[29] K. Diethelm, An algorithm for the numerical solution of differential equations of fractional order, Electronic transactions on numerical analysis 5 (1997) 1-6.
[30] M.M. Meerschaert, C. Tadjeran, Finite difference approximations for two-sided space-fractional partial differential equations, Applied Numerical Mathematics 56 (2006) 80-90.
[31] N.F. Ford, A.C. Simpson, The numerical solution of fractional differential equations: speed versus accuracy, Numerical Algorithms 26 (2001) 333-346.
[32] E.A. Rawashdeh, Numerical solution of fractional integro-differential equations by collocation method, Applied Mathematics and Computation 176 (2006) 1-6.
[33] P. Kumar, O.P. Agrawal, An approximate method for numerical solution of fractional differential equations, Signal Processing 86 (2006) 2602-2610.
[34] S. Momani, Z. Odibat, Numerical approach to differential equations of fractional order, Journal of Computational and Applied Mathematics 207 (2007) 96-110.
[35] R. Du, W.R. Cao, Z.Z. Sun, A compact difference scheme for the fractional diffusion-wave equation, Applied Mathematical Modelling 34 (2010) 2998-3007.
[36] J. Ren, Z.Z. Sun, Numerical Algorithm With High Spatial Accuracy for the Fractional Diffusion-Wave Equation With Neumann Boundary Conditions, J Sci Comput 56 (2013) 381-408.
[37] J. Huang, L. Vzquez, J. Yang, Two diffusion difference schemes for time-fractional diffusion-wave equation, Numer Algor 64 (2013) 707-720.
[38] J.Y. Yang, J.F. Huang, D.M. Liang, Y.F. Tang, Numerical solution of fractional diffusion-wave equation based on fractional multistep method, Applied Mathematical Modelling 38 (2014) 3652-3661.
[39] F. Zeng, Second-Order Stable Finite Difference Schemes for the Time-fractional Diffusion-wave Equation, J Sci Comput 65 (2015) 411-430.
[40] H. Ding, C. Li, Numerical Algorithms for the Fractional Diffusion-Wave Equation with Reaction Term, Abstract and Applied Analysis 13 (2013) Article ID 493406, 15 pages.
[41] J.Q. Murillo, S.B. Yuste, An Explicit Difference Method for Solving Fractional Diffusion and Diffusion-Wave Equation in the Caputo Form,J. Comput. Nonlinear Dynam 6 (2010) 021014 6 pages.
[42] L.L. Ferrás, N.J. Ford, M.L. Morgado, M. Rebelo, G.H. McKinley, J.M. Nóbrega, A primer on experimental and computational rheology with fractional viscoelastic constitutive models, AIP Conference Proceedings 1843, 020002 (2017); doi: 10.1063/1.4982977.

[43] N.W. Tschoegl, The phenomenological theory of linear viscoelastic behavior: an introduction. Springer Science & Business Media, 2012.
[44] B. Keshavarz, T. Divoux, S. Manneville, G.H. McKinley, Nonlinear viscoelasticity and generalized failure criterion for biopolymer gels, accepted for publication in Physical Review Letters (2016).
[45] T.S.K. Ng, G.H. McKinley, M. Padmanabhan, Linear to non-linear rheology of wheat flour dough, Appl Rheol 16 (2006) 265274
[46] M. Caputo, Elasticità e Dissipazione , Zanichelli, Bologna, Italy, 1969.
[47] K. Diethelm, The analysis of fractional differential equations: An application-oriented exposition using differential operators of Caputo type, Springer, Heidelberg, New York, 2010.
[48] G.W. Scott-Blair, The role of psychophysics in rheology, J. Colloid Science 2 (1947) 21-32.
[49] R.C. Koeller, Applications of fractional calculus to the theory of viscoelasticity, Journal of Applied Mechanics 51 (1984) 299-307.
[50] H. Schiessel, A. Blumen, Hierarchical analogues to fractional relaxation equations, Journal of Physics A: Mathematical and General 26 (1993) 5057-5069.
[51] H. Schiessel, R. Metzler, A. Blumen, T.F. Nonnenmacher, Generalized viscoelastic models: their fractional equations with solutions, Journal of physics A: Mathematical and General 28 (1995) 6567-6584.
[52] H. Schiessel, P. Alemany, A. Blumen, Dynamics in disordered systems, Progr. Colloid. Polym. Sci. 96 (1994) 16-21.
[53] A.G. Jiménez, B.V. Jara, J.H. Santiago, Relaxation modulus in the fitting of polycarbonate and poly(vinyl chloride) viscoelastic polymers by a fractional Maxwell model, Colloid Polymer Science 280 (2002) 485-489.
[54] A.G. Jiménez, J.H. Santiago, A.M. García, J.S. González, Relaxation modulus in PMMA and PTFE fitting by fractional Maxwell model, Polymer Testing 21 (2002) 325-331.
[55] C.W. Macosko, Rheology: Principles, Measurements, and Application, VCH: New York, 1994.
[56] O.S. Carneiro, L.L. Ferrás, P. Teixeira, C. Fernandes, J.M. Nóbrega, AIP Conf. Proc. 1662 (2015) 030012.
[57] M.P.F Costa, C.P.B. Ribeiro, Generalized fractional Maxwell model: Parameter estimation of a viscoelastic material, in 10th International Conference of Numerical Analysis and Applied Mathematics, edited by Theodore E. Simos, George Psihoyios, Ch. Tsitouras, Zacharias Anastassi (Eds.), AIP Conference Proceedings 1479 (2012) 790-793.
[58] H. Jeffreys, The Earth, Cambridge University Press (1995) 265-.
[59] G.A. Holzapfel, Nonlinear solid mechanics, Vol. 24. Chichester, Wiley, 2000.
[60] J.N. Reddy, An Introduction to Continuum Mechanics, Cambridge University Press, 2013.
[61] C. Truesdell, W. Noll, The Non-Linear Field Theories of Mechanics/Die Nicht-Linearen Feldtheorien der Mechanik, Vol. 2 Springer Science & Business Media, 2013.
[62] D.D. Joseph, Fluid dynamics of viscoelastic liquids, Vol. 84 Springer Science & Business Media, 2013.
[63] A. Morozov, S.E. Spagnolie, Introduction to complex fluids, Complex Fluids in Biological Systems, Springer New York, 2015, 3-52.
[64] P. Yang, Y. Cheong Lam, Ke-Qin Zhu, Constitutive equation with fractional derivatives for the generalized UCM model, J. Non-Newt. Fluid Mech. 165 (2010) 88-97.
[65] J.G. Oldroyd, On the formulation of rheological equations of state, Proc. Roy. Soc. A 200 (1950) 523-541.
[66] A.S. Lodge,On the use of convected coordinate systems in the mechanics of continuous media, Proc. Camb. Phil. Soc. 47 (1951) 575-584.
[67] R.R. Huilgol, Continuum mechanics of viscoelastic liquids, New York: Halsted Press, 1975.
[68] R.R. Huilgol, N. Phan-Thien, Fluid mechanics of viscoelasticity: general principles, constitutive modelling and numerical techniques, Rheology series vol. 6, 1997.
[69] A.C. Pipkin, Lectures on Viscoelastic Theory , Springer, New York, 1972.
[70] X. Huang, N. Phan-Thien, R. Tanner, Viscoelastic flow between eccentric rotating cylinders: unstructured control volume method, Journal of non-newtonian fluid mechanics 64 (1996) 71-92.
[71] R. Kupferman, Simulation of Viscoelastic Fluids: Couette-Taylor Flow, Journal of Computational Physics 147 (1998) 22-59.
[72] R. Larson, Instabilities in viscoelastic flows, Rheologica Acta 31 (1992) 213-263.
[73] M. Norouzi, M. Sedaghat, M. Shahmardan, M. Nobari, On the origin of viscoelastic Taylor-Couette instability resulted from normal stress differences, Korea-Australia Rheology Journal 27 (2015) 41-53.
[74] J.M. Piau, M. Bremond, J.M. Couette, M. Piau, Maurice Couette, one of the founders of rheology, Rheologica acta 33 (1994) 357-368.
[75] R.J. Donnelly, TaylorCouette flow: The early days, Phys. Today 44 (1991) 3239
[76] P. Dontula, C.W. Macosko, L.E. Scriven, Origins of concentric cylinders viscometry, Journal of Rheology 49

(2005) 807-818.
[77] P.J. Roache, Code Verification by the Method of Manufactured Solutions, Trans. ASME, J. Fluids Engineering 124 (2002) 4-10.
[78] K. Salari, P. Knupp, Code Verification by the Method of Manufactured Solutions, Sandia Report, Sandia National Laboratories, 2000.
[79] P.A.M. Dirac, The Principles of Quantum Mechanics, 3rd ed., Oxford University Press, 1947.
[80] C. Friedrich, Relaxation and retardation functions of the Maxwell model with fractional derivatives, Rheologica Acta 30 (1991) 151-158.
[81] Y.N. Zhang, Z.Z. Sun, H.L. Liao, Finite difference methods for the time fractional diffusion equation on non-uniform meshes, Journal of Computational Physics 265 (2014) 195-210.
[82] M.L. Morgado, M. Rebelo, Introducing graded meshes in the numerical approximation of distributed-order diffusion equations, Proceedings of the 2nd International Conference NUMERICAL COMPUTATIONS: THEORY AND ALGORITHMS (NUMTA2016), DOI: 10.1063/1.4965348.
[83] L. F. Morgado and M. L. Morgado, Numerical modelling transient current in the time-of-flight experiment with time-fractional advection-diffusion equations, Journal of Mathematical Chemistry, 53 (2015) 958 -973.
[84] M. Stynes, E. O'Riordan, J.L. Gracia, Error analysis of a finite difference method on graded meshes for a time-fractional diffusion equation.
[85] C-S Sin, L. Zheng, J-S Sin, F. Liu, L. Liu, Unsteady flow of viscoelastic fluid with the fractional K-BKZ model between two parallel plates, Applied Mathematical Modelling 47 (2017) 114-127.
[86] K.R. Rajagopal, R.K. Bhatnagar, Exact solutions for some simple flows of an Oldroyd-B fluid, Acta Mechanica 113 (1995) 233239.
mimimi

Appendix A. Equations governing the annular flow of an UCM fluid

The momentum conservation equations are given (in cylindrical coordinates) by (see [9] pp. 612),

$$\begin{aligned}
\rho\left(\frac{\partial u_r}{\partial t}+u_r\frac{\partial u_r}{\partial r}-\frac{u_\theta^2}{r}+u_z\frac{\partial u_r}{\partial z}\right) &= \frac{1}{r}\frac{\partial(r\sigma_{rr})}{\partial r}+\frac{\partial\sigma_{zr}}{\partial z}-\frac{\sigma_{\theta\theta}}{r}-\frac{\partial p}{\partial r}+\rho g_r\\
\rho\left(\frac{\partial u_\theta}{\partial t}+u_r\frac{\partial u_\theta}{\partial r}+\frac{u_r u_\theta}{r}+u_z\frac{\partial u_\theta}{\partial z}\right) &= \frac{1}{r^2}\frac{\partial\left(r^2\sigma_{r\theta}\right)}{\partial r}+\frac{\partial\sigma_{z\theta}}{\partial z}-\frac{1}{r}\frac{\partial p}{\partial\theta}+\rho g_\theta\\
\rho\left(\frac{\partial u_z}{\partial t}+u_r\frac{\partial u_z}{\partial r}+u_z\frac{\partial u_z}{\partial z}\right) &= \frac{1}{r}\frac{\partial(r\sigma_{rz})}{\partial r}+\frac{\partial\sigma_{zz}}{\partial z}-\frac{\partial p}{\partial z}+\rho g_z
\end{aligned} \tag{A.1}$$

where, since it was assumed that the flow is axisymmetric, $\frac{\partial}{\partial\theta}=0$.

The Upper-Convected-Maxwell model is given in cylindrical coordinates by (see [9] pp. 344, and, pp. 614):

$$\begin{aligned}
\sigma_{rr}+\lambda\frac{\partial\sigma_{rr}}{\partial t}+\lambda\left\{u_r\frac{\partial\sigma_{rr}}{\partial r}+u_z\frac{\partial\sigma_{rr}}{\partial z}-2\sigma_{rr}\frac{\partial u_r}{\partial r}-2\sigma_{rz}\frac{\partial u_r}{\partial z}\right\} &= 2\eta\frac{\partial u_r}{\partial r}\\
\sigma_{r\theta}+\lambda\frac{\partial\sigma_{r\theta}}{\partial t}+\lambda\left\{u_r\frac{\partial\sigma_{r\theta}}{\partial r}+u_z\frac{\partial\sigma_{r\theta}}{\partial z}+\sigma_{rr}\left(\frac{u_\theta}{r}-\frac{\partial u_\theta}{\partial r}\right)-\sigma_{r\theta}\left(\frac{u_r}{r}+\frac{\partial u_r}{\partial r}\right)-\sigma_{rz}\frac{\partial u_\theta}{\partial z}-\sigma_{\theta z}\frac{\partial u_r}{\partial z}\right\} &= \eta\left(\frac{\partial u_\theta}{\partial r}-\frac{u_\theta}{r}\right)\\
\sigma_{rz}+\lambda\frac{\partial\sigma_{rz}}{\partial t}+\lambda\left\{u_r\frac{\partial\sigma_{rz}}{\partial r}+u_z\frac{\partial\sigma_{rz}}{\partial z}-\sigma_{rr}\frac{\partial u_z}{\partial r}-\sigma_{rz}\left(\frac{\partial u_z}{\partial z}+\frac{\partial u_r}{\partial r}\right)-\sigma_{zz}\frac{\partial u_r}{\partial z}\right\} &= \eta\left(\frac{\partial u_z}{\partial r}+\frac{\partial u_r}{\partial z}\right)\\
\sigma_{\theta\theta}+\lambda\frac{\partial\sigma_{\theta\theta}}{\partial t}+\lambda\left\{u_r\frac{\partial\sigma_{\theta\theta}}{\partial r}+u_z\frac{\partial\sigma_{\theta\theta}}{\partial z}-2\sigma_{\theta\theta}\frac{u_r}{r}+2\sigma_{r\theta}\left(\frac{u_\theta}{r}-\frac{\partial u_\theta}{\partial r}\right)-2\sigma_{\theta z}\frac{\partial u_\theta}{\partial z}\right\} &= 2\eta\left(\frac{1}{r}\frac{\partial u_\theta}{\partial\theta}+\frac{u_r}{r}\right)\\
\sigma_{\theta z}+\lambda\frac{\partial\sigma_{\theta z}}{\partial t}+\lambda\left\{u_r\frac{\partial\sigma_{\theta z}}{\partial r}+u_z\frac{\partial\sigma_{\theta z}}{\partial z}+\sigma_{rz}\left(\frac{u_\theta}{r}-\frac{\partial u_\theta}{\partial r}\right)-\sigma_{\theta z}\left(\frac{u_r}{r}+\frac{\partial u_z}{\partial z}\right)-\sigma_{r\theta}\frac{\partial u_z}{\partial r}-\sigma_{zz}\frac{\partial u_\theta}{\partial z}\right\} &= \eta\left(\frac{1}{r}\frac{\partial u_z}{\partial\theta}+\frac{\partial u_\theta}{\partial z}\right)\\
\sigma_{zz}+\lambda\frac{\partial\sigma_{zz}}{\partial t}+\lambda\left\{u_r\frac{\partial\sigma_{zz}}{\partial r}+u_z\frac{\partial\sigma_{zz}}{\partial z}-2\sigma_{rz}\frac{\partial u_z}{\partial r}-2\sigma_{zz}\frac{\partial u_z}{\partial z}\right\} &= 2\eta\frac{\partial u_z}{\partial z}
\end{aligned} \tag{A.2}$$

where it was once again assumed that the flow is axisymmetric ($\frac{\partial}{\partial\theta}=0$). Note that the Maxwell model is recovered if $\lambda\{...\}=0$ in all six equations.

Now, assuming that we only have tangential movement, the velocity profile is given by $(u_r,u_\theta,u_z)=(0,u_\theta(r,t),0)$. This means that, for a fixed t, we can only see changes in velocity when moving in the radial direction, as shown in figure 6. With this assumption, the equations for the stress are further simplified ($u_r=u_z=0$ and $\frac{\partial}{\partial\theta}=\frac{\partial}{\partial z}=0$), being given by,

$$\begin{array}{ll}
\sigma_{rr}+\lambda\frac{\partial\sigma_{rr}}{\partial t}+\{0\} & =0\\
\sigma_{r\theta}+\lambda\frac{\partial\sigma_{r\theta}}{\partial t}+\lambda\left\{\sigma_{rr}\left(\frac{u_\theta}{r}-\frac{\partial u_\theta}{\partial r}\right)\right\} & =\eta\left(\frac{\partial u_\theta}{\partial r}-\frac{u_\theta}{r}\right)\\
\sigma_{rz}+\lambda\frac{\partial\sigma_{rz}}{\partial t}+\{0\} & =0\\
\sigma_{\theta\theta}+\lambda\frac{\partial\sigma_{\theta\theta}}{\partial t}+\lambda\left\{2\sigma_{r\theta}\left(\frac{u_\theta}{r}-\frac{\partial u_\theta}{\partial r}\right)\right\} & =0\\
\sigma_{\theta z}+\lambda\frac{\partial\sigma_{\theta z}}{\partial t}+\lambda\left\{\sigma_{rz}\left(\frac{u_\theta}{r}-\frac{\partial u_\theta}{\partial r}\right)\right\} & =0\\
\sigma_{zz}+\lambda\frac{\partial\sigma_{zz}}{\partial t}+\{0\} & =0
\end{array} \tag{A.3}$$

We have obtained three similar differential equations, represented now by $\sigma(r,t)+\lambda\frac{\partial\sigma(r,t)}{\partial t}=0$ (without the subscripts). Assuming the fluid is at rest when $t=0$ then we have $\sigma(r,0)=0$. The solution of this initial value problem is the trivial solution $\sigma(r,t)=0$ for all t (the general solution is $\sigma(r,t)=f(r)\,e^{-t/\lambda}$). Therefore the stress tensor is given by,

$$\begin{array}{ll}
\sigma_{rr}=\sigma_{rz}=\sigma_{zz}=\sigma_{\theta z} & =0\\
\sigma_{r\theta}+\lambda\frac{\partial\sigma_{r\theta}}{\partial t}+\{0\} & =\eta\left(\frac{\partial u_\theta}{\partial r}-\frac{u_\theta}{r}\right)\\
\sigma_{\theta\theta}+\lambda\frac{\partial\sigma_{\theta\theta}}{\partial t}+\lambda\left\{2\sigma_{r\theta}\left(\frac{u_\theta}{r}-\frac{\partial u_\theta}{\partial r}\right)\right\} & =0
\end{array} \tag{A.4}$$

Note that for the shear stress, $\sigma_{r\theta}$, the contribution of the upper convective derivative is null. This means that the shear stress obtained for the UCM and Maxwell models is the same, for this type of flows. Regarding the momentum equation, since it is independent of the constitutive model, it will be the same for the UCM and Maxwell models. Considering all the simplifications described before, the momentum equations can be written as:

$$\begin{array}{ll}
-\rho\frac{u_\theta^2}{r} & =-\frac{\sigma_{\theta\theta}}{r}-\frac{\partial p}{\partial r}\\
\rho\frac{\partial u_\theta}{\partial t} & =\frac{2}{r}\sigma_{r\theta}+\frac{\partial\sigma_{r\theta}}{\partial r}
\end{array} \tag{A.5}$$

where the z momentum equation was eliminated due to the absence of movement and gradients in this direction. The stress, $\sigma_{r\theta}$, and velocity, u_θ, can be fully determined using equations (A.4.2) and (A.5.2).

Note also that is possible to obtain an equation for velocity, only (this was shown in [86]). By applying $\left(1+\lambda\frac{\partial}{\partial t}\right)$ in both sides of equation (A.5.2) we obtain $\rho\left(1+\lambda\frac{\partial}{\partial t}\right)\frac{\partial u_\theta}{\partial t}=\left(\frac{2}{r}+\frac{\partial}{\partial r}\right)\left(1+\lambda\frac{\partial}{\partial t}\right)\sigma_{r\theta}$, and, applying $\left(\frac{2}{r}+\frac{\partial}{\partial r}\right)$ in both sides of equation (A.4.2) we have,

$$\left(\frac{2}{r}+\frac{\partial}{\partial r}\right)\left(1+\lambda\frac{\partial}{\partial t}\right)\sigma_{r\theta}=\eta\left(\frac{2}{r}+\frac{\partial}{\partial r}\right)\left(\frac{\partial u_\theta}{\partial r}-\frac{u_\theta}{r}\right) \tag{A.6}$$

(we have dropped the term $\{0\}$), leading to,

$$\rho\left(1+\lambda\frac{\partial}{\partial t}\right)\frac{\partial u_\theta}{\partial t}=\eta\left(\frac{2}{r}+\frac{\partial}{\partial r}\right)\left(\frac{\partial u_\theta}{\partial r}-\frac{u_\theta}{r}\right) \tag{A.7}$$

Note also that this equation is valid for both models (UCM and Maxwell).

Appendix B.
Numerical Solution of the FMM

In order to perform simulations with the FMM we need to slightly adapt the numerical method proposed before for the FVF model. Remember that the momentum equation of interest is given by (see Appendix A),

$$\rho\frac{\partial u_\theta}{\partial t}=\eta\left(\frac{2}{r}+\frac{\partial}{\partial r}\right)\sigma_{r\theta} \tag{B.1}$$

and that the FMM is given by ($\alpha>\beta$),

$$\left(1+\frac{\mathbb{V}}{\mathbb{G}}\frac{d^{\alpha-\beta}}{dt^{\alpha-\beta}}\right)\boldsymbol{\sigma}\left(t\right)=\mathbb{V}\frac{d^{\alpha}\boldsymbol{\gamma}\left(t\right)}{dt^{\alpha}}, \tag{B.2}$$

or in integral form,

$$\boldsymbol{\sigma}\left(t\right)+\frac{\mathbb{V}}{\mathbb{G}}\frac{1}{\Gamma\left(1-(\alpha-\beta)\right)}\int_0^t\left(t-t'\right)^{-(\alpha-\beta)}\frac{d\boldsymbol{\sigma}\left(t'\right)}{dt'}dt'=\mathbb{V}\frac{1}{\Gamma\left(1-\alpha\right)}\int_0^t\left(t-t'\right)^{-\alpha}\frac{d\boldsymbol{\gamma}\left(t'\right)}{dt'}dt'. \tag{B.3}$$

For the method derived before we have that $\alpha\to 1$ and therefore $\frac{d^{\alpha}\boldsymbol{\gamma}(t)}{dt^{\alpha}}$ converges to the rate of deformation, $\frac{d\boldsymbol{\gamma}(t)}{dt}$, that for this particular flow is given by $\left(\frac{\partial u_\theta}{\partial r}-\frac{u_\theta}{r}\right)$. When $\alpha\neq 1$ we need to consider all the past deformations, $\boldsymbol{\gamma}\left(t'\right)$, by computing the integral,

$$\frac{\mathbb{V}}{\Gamma\left(1-\alpha\right)}\int_0^t\left(t-t'\right)^{-\alpha}\left(\frac{\partial u_\theta(r,t')}{\partial r}-\frac{u_\theta(r,t')}{r}\right)dt'. \tag{B.4}$$

If we apply $\left(\frac{2}{r}+\frac{\partial}{\partial r}\right)$ to equation B.2 and $\left(1+\frac{\mathbb{V}}{\mathbb{G}}\frac{d^{\alpha-\beta}}{dt^{\alpha-\beta}}\right)$ to equation B.1, we obtain the following system of equations:

$$\rho\left(1+\frac{\mathbb{V}}{\mathbb{G}}\frac{d^{\alpha-\beta}}{dt^{\alpha-\beta}}\right)\frac{\partial u_\theta}{\partial t}=\frac{\mathbb{V}}{\Gamma\left(1-\alpha\right)}\int_0^t\left(t-t'\right)^{-\alpha}\left(\frac{\partial^2 u_\theta(r,t')}{\partial r^2}+\frac{1}{r}\frac{\partial u_\theta(r,t')}{\partial r}-\frac{u_\theta(r,t')}{r}\right)dt', \tag{B.5}$$

$$\left(1+\frac{\mathbb{V}}{\mathbb{G}}\frac{d^{\alpha-\beta}}{dt^{\alpha-\beta}}\right)\boldsymbol{\sigma}\left(t\right)=\frac{\mathbb{V}}{\Gamma\left(1-\alpha\right)}\int_0^t\left(t-t'\right)^{-\alpha}\left(\frac{\partial u_\theta(r,t')}{\partial r}-\frac{u_\theta(r,t')}{r}\right)dt'. \tag{B.6}$$

Note that the left-hand-side of both equations is similar to what was obtained when $\alpha\to 1$, and therefore, the discretisation presented before for $\alpha=1$ applies here (assuming that $1-\alpha$ is substituted by $\alpha-\beta$. Now, we only need to approximate the integral on the righ-hand-side of both equations.

At $t=t_s$ the integral on the right-hand side of the momentum equation can be written as,

$$\begin{aligned}&\int_0^{t_s}(t_s-t')^{-\alpha}\left(\frac{\partial^2 u_\theta(r,t')}{\partial r^2}+\frac{1}{r}\frac{\partial u_\theta(r,t')}{\partial r}-\frac{u_\theta(r,t')}{r}\right)dt'=\\&=\sum_{j=0}^{s-2}\int_{t_j}^{t_{j+1}}(t_s-t')^{-\alpha}\left(\frac{\partial^2 u_\theta(r,t')}{\partial r^2}+\frac{1}{r}\frac{\partial u_\theta(r,t')}{\partial r}-\frac{u_\theta(r,t')}{r}\right)dt'\\&+\int_{t_{s-1}}^{t_s}(t_s-t')^{-\alpha}\left(\frac{\partial^2 u_\theta(r,t')}{\partial r^2}+\frac{1}{r}\frac{\partial u_\theta(r,t')}{\partial r}-\frac{u_\theta(r,t')}{r}\right)dt'\end{aligned}\tag{B.7}$$

for $s=1,...,S$. We also know that $\frac{\partial^2 u_\theta(r,t')}{\partial r^2}+\frac{1}{r}\frac{\partial u_\theta(r,t')}{\partial r}-\frac{u_\theta(r,t')}{r}$ can by approximated by $\delta_r^2 u_i^{s-1/2}+\frac{1}{2r_i}\left(\frac{\delta_r u_i^s+\delta_r u_i^{s-1}}{2}\right)-\frac{u_i^{s-1/2}}{r_i^2}$ for each time step s. Therefore, we have,

$$\begin{aligned}&\tfrac{\mathbb{V}}{\Gamma(1-\alpha)}\int_0^{t_s}(t_s-t')^{-\alpha}\left(\frac{\partial^2 u_\theta(r,t')}{\partial r^2}+\frac{1}{r}\frac{\partial u_\theta(r,t')}{\partial r}-\frac{u_\theta(r,t')}{r}\right)dt'\approx\\&\approx\sum_{j=0}^{s-2}\left[\left(\delta_r^2 u_i^{(j+1)-1/2}+\frac{1}{2r_i}\left(\frac{\delta_r u_i^{(j+1)}+\delta_r u_i^{(j+1)-1}}{2}\right)-\frac{u_i^{(j+1)-1/2}}{r_i^2}\right)\tfrac{\mathbb{V}}{\Gamma(1-\alpha)}\int_{t_j}^{t_{j+1}}(t_s-t')^{-\alpha}dt'\right]\\&+\mathbb{V}\left(\delta_r^2 u_i^{s-1/2}+\frac{1}{2r_i}\left(\frac{\delta_r u_i^s+\delta_r u_i^{s-1}}{2}\right)-\frac{u_i^{s-1/2}}{r_i^2}\right)\tfrac{1}{\Gamma(1-\alpha)}\int_{t_{s-1}}^{t_s}(t_s-t')^{-\alpha}dt'\end{aligned}\tag{B.8}$$

Since $\int_{t_{s-1}}^{t_s}(t_s-t')^{-\alpha}dt'=\frac{\Delta t^{1-\alpha}}{1-\alpha}$ and $\int_{t_j}^{t_{j+1}}(t_s-t')^{-\alpha}dt'=\frac{\Delta t^{1-\alpha}d_{sj}}{1-\alpha}$ the final result is given by:

$$\begin{aligned}&\tfrac{\mathbb{V}}{\Gamma(1-\alpha)}\int_0^{t_s}(t_s-t')^{-\alpha}\left(\frac{\partial^2 u_\theta(r,t')}{\partial r^2}+\frac{1}{r}\frac{\partial u_\theta(r,t')}{\partial r}-\frac{u_\theta(r,t')}{r}\right)dt'\approx\\&\approx\tfrac{\mathbb{V}\Delta t^{1-\alpha}}{\Gamma(2-\alpha)}\sum_{j=0}^{s-2}\left[\left(\delta_r^2 u_i^{(j+1)-1/2}+\frac{1}{2r_i}\left(\frac{\delta_r u_i^{(j+1)}+\delta_r u_i^{(j+1)-1}}{2}\right)-\frac{u_i^{(j+1)-1/2}}{r_i^2}\right)d_{sj}\right]\\&+\tfrac{\mathbb{V}\Delta t^{1-\alpha}}{\Gamma(2-\alpha)}\left(\delta_r^2 u_i^{s-1/2}+\frac{1}{2r_i}\left(\frac{\delta_r u_i^s+\delta_r u_i^{s-1}}{2}\right)-\frac{u_i^{s-1/2}}{r_i^2}\right)\end{aligned}\tag{B.9}$$

with $d_{sj}=\left[(s-j)^{1-\alpha}-(s-(j+1))^{1-\alpha}\right]$.

This means that the new numerical method to solve the momentum equation is given by

$$\begin{aligned}&\tfrac{\rho}{\mathbb{V}}\delta_t u_i^{s-1/2}+\tfrac{\rho}{\Gamma(\{1-(\alpha-\beta)\})\mathbb{G}}\tfrac{1}{\Delta t}\left[a_0\delta_t u_i^{s-1/2}-\sum_{j=0}^{s-1}\left(a_{n-j-1}-a_{n-j}\right)\delta_t u_i^{j-1/2}\right]\\&-\left\{\tfrac{\Delta t^{1-\alpha}}{\Gamma(2-\alpha)}\right\}\left(\delta_r^2 u_i^{s-1/2}+\frac{1}{2r_i}\left(\frac{\delta_r u_i^s+\delta_r u_i^{s-1}}{2}\right)-\frac{u_i^{s-1/2}}{r_i^2}\right)\\&=\left\{\tfrac{\Delta t^{1-\alpha}}{\Gamma(2-\alpha)}\sum_{j=0}^{s-2}\left[\left(\delta_r^2 u_i^{(j+1)-1/2}+\frac{1}{2r_i}\left(\frac{\delta_r u_i^{(j+1)}+\delta_r u_i^{(j+1)-1}}{2}\right)-\frac{u_i^{(j+1)-1/2}}{r_i^2}\right)d_{sj}\right]\right\}\end{aligned}\tag{B.10}$$

for $i=1,...,N-1$ and $s=1,...,S$. We only need to add the terms in $\{...\}$ to the original code (equation 23). Also, we now have,

$$a_l=\int_{t_l}^{t_{l+1}}\frac{1}{t^{\epsilon-1}}dt=\frac{(\Delta t)^{2-\epsilon}}{2-\epsilon}\left[(l+1)^{2-\epsilon}-l^{2-\epsilon}\right],\ l\geq 0.\tag{B.11}$$

and $\epsilon=1+\alpha-\beta$.

For the numerical solution of the stress equation we need to perform a similar approximation to the right-hand-side integral, the only difference is that we now have all the velocity profiles up to the actual time step, and therefore the following approximation can be used:

$$\begin{aligned}\tfrac{\mathbb{V}}{\Gamma(1-\alpha)}\int_0^{t_s}(t_s-t')^{-\alpha}\left(\frac{\partial u_\theta(r,t')}{\partial r}-\frac{u_\theta(r,t')}{r}\right)dt'\approx\ &\tfrac{\mathbb{V}\Delta t^{1-\alpha}}{\Gamma(2-\alpha)}\sum_{j=0}^{s-2}\left[\left(\frac{u_{i+1}^{j+1}-u_{i-1}^{j+1}}{2\Delta r}-\frac{u_i^{j+1}}{r_i}\right)d_{sj}\right]\\&+\tfrac{\mathbb{V}\Delta t^{1-\alpha}}{\Gamma(2-\alpha)}\left[\tfrac{u_{i+1}^s-u_{i-1}^s}{2\Delta r}-\tfrac{u_i^s}{r_i}\right]\end{aligned}\tag{B.12}$$

Then, the discretised shear stress equation can written as:

$$\sigma_i^s + \frac{\mathbb{V}}{\Gamma(\{1-(\alpha-\beta)\})\mathbb{G}} \frac{1}{\Delta t} \left[b_0 \sigma_i^s - \sum_{j=0}^{s-1} \left(b_{n-j-1} - b_{n-j} \right) \sigma_i^j \right] = \left\{ \frac{\mathbb{V} \Delta t^{1-\alpha}}{\Gamma(2-\alpha)} \sum_{j=0}^{s-2} \left[\left(\frac{u_{i+1}^{j+1} - u_{i-1}^{j+1}}{2\Delta r} - \frac{u_i^{j+1}}{r_i} \right) d_{sj} \right] \right\} + \left\{ \frac{\Delta t^{1-\alpha}}{\Gamma(2-\alpha)} \right\} \mathbb{V} \left(\frac{u_{i+1}^s - u_{i-1}^s}{2\Delta r} - \frac{u_i^s}{r_i} \right) \tag{B.13}$$

for $i = 1, ..., N-1$ and $s = 1, ..., S$ with,

$$b_l = \int_{t_l}^{t_{l+1}} \frac{1}{t^\Theta} dt = \frac{(\Delta t)^{1-\Theta}}{1-\Theta} \left[(l+1)^{1-\Theta} - l^{1-\Theta} \right], \; l \geq 0. \tag{B.14}$$

and $\Theta = \alpha - \beta$. Again, we only need to add the terms in $\{...\}$ to the original code (equation 24).

The code can be extended to deal with graded meshes. In that case, the definitions of a_l, b_l and d_{sj} make no sense, since they were obtained assuming a uniform mesh. The extended numerical method to solve the momentum equation is then given by

$$\begin{aligned} &\frac{\rho}{\mathbb{V}} \delta_{tgrad} u_i^{s-1/2} + \frac{\rho}{\Gamma(\{1-(\alpha-\beta)\})\mathbb{G}} \left[\frac{a_{s,s}}{\Delta t[s]} \left(\delta_{tgrad} u_i^{s-1/2} - \delta_{tgrad} u_i^{(s-1)-1/2} \right) \right] \\ &\quad - \frac{\rho}{\Gamma(\{1-(\alpha-\beta)\})\mathbb{G}} \left[\sum_{j=0}^{s-1} \left(\frac{a_{s,j+1}}{\Delta t[j+1]} \left(\delta_{tgrad} u_i^{(j+1)-1/2} - \delta_{tgrad} u_i^{(j)-1/2} \right) \right) \right] \\ &\quad - \left\{ \frac{\Delta t[s]^{1-\alpha}}{\Gamma(2-\alpha)} \right\} \left(\delta_r^2 u_i^{s-1/2} + \frac{1}{2r_i} \left(\frac{\delta_r u_i^s + \delta_r u_i^{s-1}}{2} \right) - \frac{u_i^{s-1/2}}{r_i^2} \right) \\ &= \left\{ \frac{1}{\Gamma(2-\alpha)} \sum_{j=0}^{s-2} \left[\left(\delta_r^2 u_i^{(j+1)-1/2} + \frac{1}{2r_i} \left(\frac{\delta_r u_i^{(j+1)} + \delta_r u_i^{(j+1)-1}}{2} \right) - \frac{u_i^{(j+1)-1/2}}{r_i^2} \right) d_{sjgrad} \right] \right\} \end{aligned} \tag{B.15}$$

for $i = 1, ..., N-1$ and $s = 1, ..., S$, with $\Delta t[s] = t_s - t_{s-1}$, $d_{sjgrad} = \left[(t_s - t_j)^{1-\alpha} - (t_s - t_{j+1})^{1-\alpha} \right]$, $\delta_{tgrad} u_i^{s-1/2} \equiv \frac{1}{\Delta t[s]} \left(u_i^s - u_i^{s-1} \right)$ and,

$$a_{s,k} = \frac{1}{2-\epsilon} \left[(t_s - t_{k-1})^{2-\epsilon} - (t_s - t_k)^{2-\epsilon} \right]. \tag{B.16}$$

The extended numerical method to solve the discretised stress equation can be written as

$$\begin{aligned} \sigma_i^s + \frac{\mathbb{V}}{\Gamma(\{1-(\alpha-\beta)\})\mathbb{G}} \frac{1}{\Delta t} \left[b_{l,l} \left(\frac{\sigma_i^s - \sigma_i^{s-1}}{\Delta t[s]} \right) - \sum_{j=0}^{s-1} b_{l,j+1} \left(\frac{\sigma_i^{j+1} - \sigma_i^j}{\Delta t[j+1]} \right) \right] = \\ = \left\{ \frac{1}{\Gamma(2-\alpha)} \sum_{j=0}^{s-2} \left[\left(\frac{u_{i+1}^{j+1} - u_{i-1}^{j+1}}{2\Delta r} - \frac{u_i^{j+1}}{r_i} \right) d_{sjgrad} \right] \right\} \\ + \left\{ \frac{\Delta t[s]^{1-\alpha}}{\Gamma(2-\alpha)} \right\} \mathbb{V} \left(\frac{u_{i+1}^s - u_{i-1}^s}{2\Delta r} - \frac{u_i^s}{r_i} \right) \end{aligned} \tag{B.17}$$

for $i = 1, ..., N-1$ and $s = 1, ..., S$ with,

$$b_{s,k} = \frac{1}{1-\Theta} \left[(t_s - t_{k-1})^{1-\Theta} - (t_s - t_k)^{1-\Theta} \right]. \tag{B.18}$$